UNIVERSITY OF ALBERTA

Mapping of Aeolian Dune Boundaries in Southern Alberta Using Landsat Thematic Mapper Data for a Wet and a Dry Period

by

Laurel Lee Murphy ©

A THESIS

SUBMITTED TO THE FACULTY OF GRADUATE STUDIES AND RESEARCH IN PARTIAL FULFILMENT OF THE REQUIREMENTS FOR THE DEGREE OF

Master of Science

Department of Earth and Atmospheric Sciences

Edmonton, Alberta

Spring, 1997

National Library of Canada
Acquisitions and Bibliographic Services
395 Wellington Street
Ottawa ON K1A 0N4
Canada

Bibliothèque nationale du Canada
Acquisitions et services bibliographiques
395, rue Wellington
Ottawa ON K1A 0N4
Canada

Your file Votre référence

Our file Notre référence

The author has granted a non-exclusive licence allowing the National Library of Canada to reproduce, loan, distribute or sell copies of his/her thesis by any means and in any form or format, making this thesis available to interested persons.

The author retains ownership of the copyright in his/her thesis. Neither the thesis nor substantial extracts from it may be printed or otherwise reproduced with the author's permission.

L'auteur a accordé une licence non exclusive permettant à la Bibliothèque nationale du Canada de reproduire, prêter, distribuer ou vendre des copies de sa thèse de quelque manière et sous quelque forme que ce soit pour mettre des exemplaires de cette thèse à la disposition des personnes intéressées.

L'auteur conserve la propriété du droit d'auteur qui protège sa thèse. Ni la thèse ni des extraits substantiels de celle-ci ne doivent être imprimés ou autrement reproduits sans son autorisation.

0-612-21195-9

Canada

University of Alberta

Library Release Form

Name of Author: Laurel Lee Murphy

Title of Thesis: Mapping of Aeolian Dune Boundaries in Southern Alberta Using Landsat Thematic Mapper Data for a Wet and a Dry Period

Degree: Master of Science in Earth and Atmospheric Sciences

Year this Degree Granted: 1997

Permission is hereby granted to the University of Alberta Library to reproduce single copies of this thesis and to lend or sell such copies for private, scholarly, or scientific research purposes only.

The author reserves all other publication and other rights in association with the copyright in the thesis, and except as hereinbefore provided, neither the thesis nor any substantial portion thereof may be printed or otherwise reproduced in any material form whatever without the author's prior written permission.

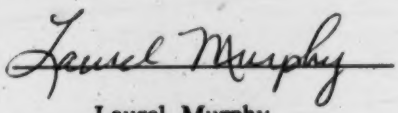

Laurel Murphy
4727 44 Avenue
Bonnyville, AB
T9N 1N6

December 11, 1996

University of Alberta

Faculty of Graduate Studies and Research

The undersigned certify that they have read, and recommend to the Faculty of Graduate Studies and Research for acceptance, a thesis entitled **Mapping of Aeolian Dune Boundaries in Southern Alberta Using Landsat Thematic Mapper Data for a Wet and a Dry Period** in partial fulfillment of the requirements for the degree of **Master of Science** in **Earth and Atmospheric Sciences**.

Dr. I. A. Campbell

Prof. A. E. Peterson

Dr. B. Rivard

9 Dec '96

Approval Date:

ABSTRACT

Multitemporal satellite data for a wet period and a dry period was used to map aeolian sand dune and interdune areas in the Duchess Dune Field, southern Alberta. Principal Component Analysis (PCA) revealed that the main temporal differences were represented in principal components 4, 5, and 6. A colour composite using these principal components effectively showed dune boundaries and dune form (parabolic). In addition to PCA, a multitemporal classification was performed; a K-means cluster analysis (unsupervised training field sampling) showed that 15 clusters or groups best represented the data. After a discriminant analysis was performed and the results interpreted, 15 original classes were merged into 7. Of these 7 classes, two aeolian deposit classes resulted which were aeolian dune areas and interdune and sand sheet areas.

ACKNOWLEDGEMENTS

The writing of this thesis was not a solitary effort and I must thank many people. I would like to thank Ron Eyton and Ian Campbell for the time and effort they contributed throughout my research. I truly appreciate Ian Campbell's patience for my jokes and Ron Eyton's Texas hospitality. I would like to thank Art Petersen and Ben Rivard, the members on my examining committee. I would also like to thank Ed Jackson who helped to make my trip to Texas possible, the Department of Earth and Atmospheric Sciences for financial assistance, and Darren Sjogren for his editing contribution.

Of course I cannot forget to thank my family for without them I would not have been able to spend so much money on tuition. I would like to thank my grandparents who helped me financially and never gave up hope that I would finish university one day. I guess they never realized I would be in University for nine years. I would like to thank my parents and siblings who never doubted my capabilities. I just wish they were capable of sending me on a trip to show their appreciation. I must also thank my colleagues and fellow partners in crime (Celina Campbell and Melodie Sept) as well as my two stepping friend Kim Miller, who was always interested in my progress and more importantly, country music.

I dedicate this thesis to the memory of Leo Lessard who was a great dance partner and a friend. He will be missed dearly.

TABLE OF CONTENTS

Mapping of Aeolian Dune Boundaries in Southern Alberta Using Landsat Thematic Mapper Data for a Wet and a Dry Period

CHAPTER

1. INTRODUCTION 1

Objectives 1

Background 3

2. MULTITEMPORAL PROCESSING 7

Spectral versus temporal signatures 7

Change detection 12

Classification through time 16

3. STUDY SITE AND IMAGE SELECTION 18

Study site 18

Image selection 21

4. MULTITEMPORAL IMAGE PROCESSING AND INTERPRETATION 26

Image registration 26

Principal Components Analysis (PCA) 27

Multitemporal eigen images and composites 28

Interpretation 31

TABLE OF CONTENTS

5. MULTITEMPORAL IMAGE CLASSIFICATION AND ANALYSIS 41

Classification 41

Multitemporal classification 44

Analysis 51

Ground truthing 59

6. SUMMARY 66

REFERENCES 68

List of Tables

Page

Table 3.1. Path and Track Information for the Wet Period and the Dry Period Satellite Data. 23

Table 4.1. Eigenvalue Report for the 12 Principal Components Generated From Raw Data for the Wet and the Dry Year. 29

Table 4.2. Eigenvector Loadings for the 12 Principal Components Generated From Raw Data for the Wet Year and the Dry Year. 30

Table 4.3. Principal Component Analysis Interpretation of the 12 Principal Components Generated for Raw Data for the Wet Year and the Dry Year. 32

Table 4.4. Four Colour Composite Eigen Images Generated Using Principal Component Analysis. 36

List of Figures

Page

Figure 1.1. Location of the Duchess dune field in southern Alberta 2
Three aeolian dune areas are present (after Shetsen 1987).

Figure 2.1. Typical spectral reflectance signature for vegetation 8
(Lillesand and Kiefer, Fig. 1.10 1994).

Figure 2.2. False colour composite of the Duchess dune field in 10
southern Alberta. TM4 (infrared 1) was assigned to
the red gun, TM3 (red) was assigned to the green gun,
and TM2 (green) was assigned to the blue gun.

Figure 2.3. Multitemporal composite colour interpretation key 11
for a 3 date multitemporal image (after Eyton 1983).

Figure 3.1. Map of the Duchess dune field showing the relationship..... 19
of aeolian and other surficial deposits (after Shetsen 1987).

Figure 3.2. Parabolic dunes in the Duchess dune field. Mean..... 20
crest to trough height variation is approximately 5 m.

Figure 3.3. Typical small blow-out area (approximately 6 m in..... 20
length and 2 m in height).

Figure 3.4. Departures from 1961-1990 mean annual precipitation..... 22
(mm) for Medicine Hat (Proudfoot 1994).

Figure 3.5. Registered Landsat TM footprint showing main areas of..... 25
the Duchess dune field.

Figure 4.1. Image I is a brightness PC image including vegetation..... 33
dynamics that was generated by assigning PC1 to the
red gun, PC2 to the green gun, PC3 to the blue gun. Area
`A' represents dune-free prairie grassland, area `B'
represents aeolian dune deposits, and area `C' represents
irrigated areas.

Figure 4.2. Image II is a temporal PC image generated by assigning 33
PC4 to the red gun, PC5 to the green gun, and PC6 to the
blue gun. See Figure 4.1 for explanation of area `A', `B',
and `C'.

List of Figures

Page

Figure 4.3. Image III is a temporal PC image for the visible and the infrared bands generated by assigning PC7 to the red gun, PC8 to the green gun, and PC9 to the blue gun. See Figure 4.1 for explanation of areas `A' to `C'. 34

Figure 4.4. Image IV is a temporal PC image showing small temporal contrasts generated by assigning PC10 to the red gun, PC11 to the green gun, and PC12 to the blue gun. See Figure 4.1 for explanation of areas `A', `B', and `C'. 34

Figure 5.1. Three types of classifiers used in the classification of image data. 43

Figure 5.2. F-ratio plot generated using cluster analysis combining Thematic Mapper data for both the wet year and the dry year. 45

Figure 5.3a. Single theme map for class 1 showing the Red Deer River and lakes. 46

Figure 5.3b. Mean grey level values for the wet year and the dry year for raw data comprising class 1. 46

Figure 5.4a. Single theme map for class 2 showing floodplain vegetation. 46

Figure 5.4b. Mean grey level values for the wet year and the dry year for raw data comprising class 2. 46

Figure 5.5a. Single theme map for class 3 showing the aeolian dunes associated with dune crest vegetation. 46

Figure 5.5b. Mean grey level values for the wet year and the dry year for raw data comprising class 3. 46

Figure 5.6a. Single theme map for class 4 showing the aeolian dunes associated with dune trough vegetation. 47

Figure 5.6b. Mean grey level values for the wet year and the dry year for raw data comprising class 4. 47

List of Figures

Page

Figure 5.7a. Single theme map for class 5 showing the vegetation associated with the Red Deer River and lakes. 47

Figure 5.7b. Mean grey level values for the wet year and the dry year for raw data comprising class 5. 47

Figure 5.8a. Single theme map for class 6 showing vegetation associated with sloping terrain near the Red Deer River and lakes. 47

Figure 5.8b. Mean grey level values for the wet year and the dry year for raw data comprising class 6. 47

Figure 5.9a. Single theme map for class 7 showing the vegetation associated with valley sides of the Red Deer River and and lakes. 48

Figure 5.9b. Mean grey level values for the wet year and the dry year for raw data comprising class 7. 48

Figure 5.10a. Single theme map for class 8 showing irrigated areas 48

Figure 5.10b. Mean grey level values for the wet year and the dry year for raw data comprising class 8. 48

Figure 5.11a. Single theme map for class 9 showing saline deposits associated with lakes. 48

Figure 5.11b. Mean grey level values for the wet and the dry year for raw data comprising class 9. 48

Figure 5.12a. Single theme map for class 10 showing dune-free prairie grasslands. 49

Figure 5.12b. Mean grey level values for the wet and the dry year for raw data comprising class 10. 49

Figure 5.13a. Single theme map for class 11 showing asphalt roads, exposed bedrock, and some blow-out dune areas. 49

List of Figures

Page

Figure 5.13b. Mean grey level values for the wet and the dry year for raw data comprising class 11. 49

Figure 5.14a. Single theme map for class 12 showing vegetation associated with a thin soil layer and near soil bedrock exposure. 49

Figure 5.14b. Mean grey level values for the wet and the dry year for raw data comprising class 12. 49

Figure 5.15a. Single theme map for class 13 showing irrigated areas 50

Figure 5.15b. Mean grey level values for the wet and the dry year for raw data comprising class 13. 50

Figure 5.16a. Single theme map for class 14 showing vegetation associated with interdune areas and cereal crops. 50

Figure 5.16b. Mean grey level values for the wet and the dry year for raw data comprising class 14. 50

Figure 5.17a. Single theme map for class 15 showing the aeolian deposits associated with vegetation. 50

Figure 5.17b. Mean grey level values for the wet and the dry year for raw data comprising class 15. 50

Figure 5.18. Map of the Duchess dune field with 15 classes (based on cluster analysis and discriminant analysis results). 54

Figure 5.19a. Classified map of the Duchess dune field created using multitemporal Landsat TM data obtained for a wet period and a dry period. Areas `A' to `E' correspond to ground photo and oblique aerial photo locations. 58

Figure 5.19b. Ground truthing guide for the satellite map (Figure 5.19a) of the Duchess dune field using oblique aerial photos and ground photos. 57

List of Figures

Page

Figure 5.20. Oblique aerial photo showing area of major aeolian dune deposition. Area 1 shows the aeolian dunes and area 2 is a blow-out area. Wind direction at time of dune formation was from the northwest (top left corner). 60

Figure 5.21. Ground photo of dune crest (area 1) and dune trough (area 2) vegetation with central blow-out (area 3) area. 60

Figure 5.22. Ground photo showing the difference between dune vegetation and interdune vegetation. The colour change in area 1 shows the transition from dune to interune areas. 61

Figure 5.23. Oblique aerial photo showing floodplain vegetation (area 1), dense tree cover (area 2), exposed to near-exposed bedrock (area 3), and the Red Deer River (area 4). 61

Figure 5.24. Ground photo of dense river vegetation (corresponds to area 2 on Figure 5.23). 63

Figure 5.25. Oblique aerial photo of lakes and associated vegetation 63

Figure 5.26. Oblique aerial photo of center pivot irrigation system 64

Figure 5.27. Dune-free prairie grasslands associated with non-sandy deposits. 64

Figure 5.28. Ground photo of gravel covered, dune-free prairie grassland vegetation areas. 65

CHAPTER 1 INTRODUCTION

The purpose of this research is to identify a satellite image processing technique suitable for mapping the distribution of aeolian deposits and moisture controlled variations in their vegetation cover, in the Duchess dune field of southern Alberta (Figure 1.1). The image processing techniques used in this research may assist mapping procedures for similar aeolian areas in Alberta and western Canada and lead to a better understanding of the distribution and changes in aeolian dunes and their response to moisture-related effects of climatic variations.

Objectives

The principal objective of this research was to identify and map the distribution of aeolian sand dunes using Landsat Thematic Mapper (TM) data collected for a wet period and a dry period. It is hypothesized that Landsat TM data will be more effective for mapping large aeolian features (*i.e.* sand sheets) and that spectral information will help delineate natural boundaries occurring between different surface features.

The specific objectives are:

1. To differentiate between aeolian and non-aeolian deposits by generating multitemporal principal component images for Landsat Thematic Mapper data for all bands of a wet period and a dry period.

2. To identify changes in the spectral signatures of vegetated aeolian deposits for a wet year and a dry year by generating a multitemporal classified image.

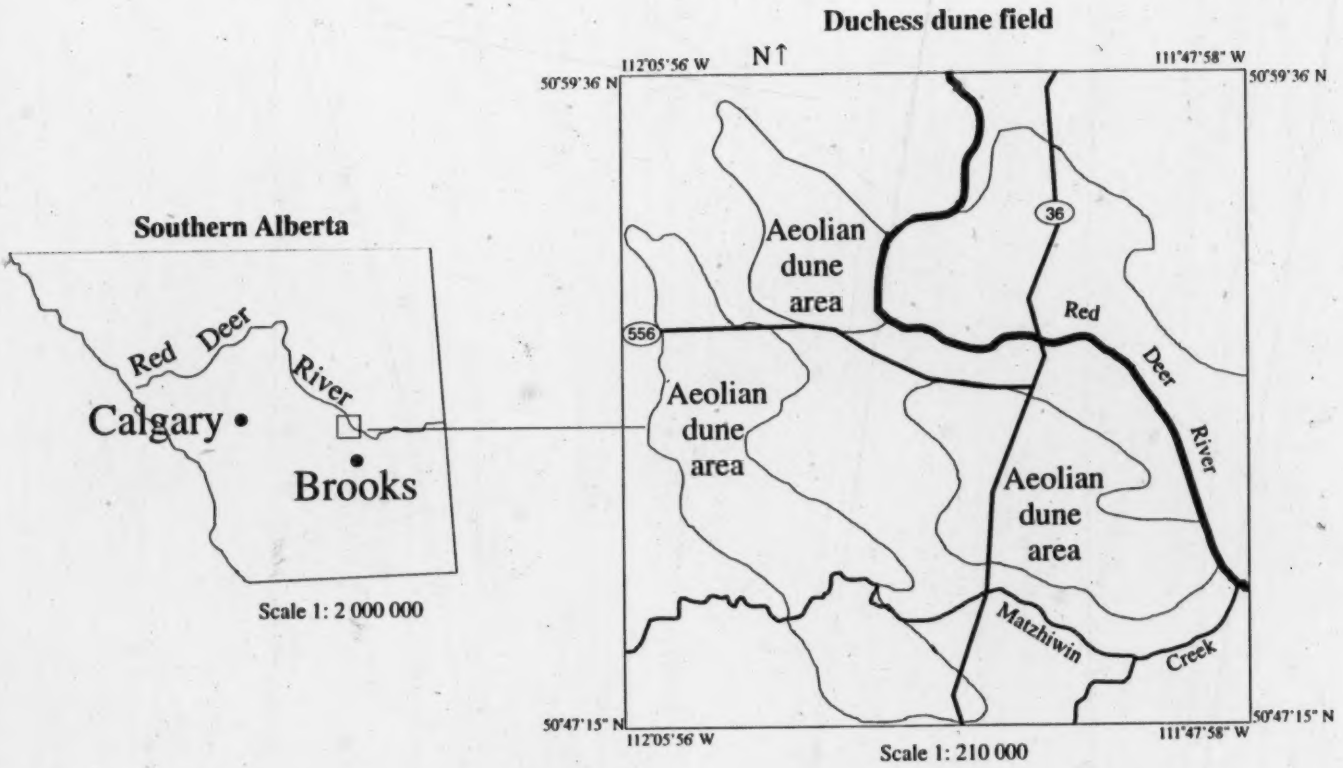

Figure 1.1. Location of the Duchess dune field in southern Alberta. Three aeolian dune areas are present (after Shetsen 1987).

3. To map the aeolian deposits based on the results of the remote sensing analyses.

Following the satellite data analysis, the distribution and characteristics of aeolian deposits in the Duchess dune field were verified on the ground and from oblique aerial photos.

Background

About 5% of the earth's land area is covered by aeolian dunes, sand sheets, and loess (Thomas 1989). Early research (*e.g.* Bagnold 1941) concentrated on the processes of dune formation and morphology. Recently, the processes involved in dune field expansion have become important due to the increasing human population in arid areas and the potential threat of dune destabilization as a result of global climatic changes (Thomas 1989).

Prior to the 1970s, environmental scientists were able to monitor and describe changes in arid zones using aerial photography and field survey techniques. During the 1970s, the availability of satellite imagery and other data provided an improved capability for describing change in arid zones; McKee and Breed (1974) used Skylab 4 photography and Landsat 1 satellite imagery to locate, identify, and map aeolian sand dune deposits in five major desert sand seas.

In Alberta, David (1977), Mulira (1986) and Shetsen (1987) mapped aeolian deposits using aerial photography and field surveys supplemented by maps of surficial geology and soil. At present there has been no attempt to map Alberta dune deposits using satellite data. David (1977) mapped areas containing aeolian dunes in Alberta that exceeded 16 km^2 in surface area but not all dunes

meeting this criteria were mapped because of the large number of dune occurrences in Alberta; for example, the Duchess dune field was omitted. Mulira (1986) mapped and evaluated the various aeolian landform types in Alberta that were at least 10 km^2 in surface area. Mulira (1986) noted the presence of aeolian sand sheet deposits, but the distribution of sand sheets was not mapped due to their widespread frequency and mobility. Shetsen (1987) used air photos, soil information, and existing surficial geology maps to define the boundaries of aeolian fields. The amount of detail and the distribution of the dunes as mapped by Shetsen (1987) differed from those mapped by David (1977) and Mulira (1986).

Limitations (*i.e.* omission of large aeolian areas and differences in the amount of detail) of the techniques used by David (1977), Mulira (1986) and Shetsen (1987) can be partially overcome using Landsat TM data. Landsat TM data are well suited to the mapping of the aeolian deposits because the satellite images cover larger areas than aerial photographs which facilitates mapping of extensive surface features such as sand sheets. Additionally, satellite data include spectral information that helps delineate natural boundaries between different surface features. These advantages are somewhat offset by the fact that air photos have higher resolution and better detail than satellite data. Nevertheless, the smaller scale of images produced using satellite data allows for the mapping of large areas which is a central theme of this research.

According to Melton (1940), Smith (1953), and David (1977) moisture

availability and the presence of vegetation are useful indicators for the distribution of aeolian dunes. David (1977) notes that vegetation does not directly cause the development of phytogenic dunes (vegetation controlled); rather the presence of vegetation is a manifestation of surface moisture which may be a more important factor. Following the suggestions of David (1977), the identification of aeolian dunes in Alberta for this research is based on the temporal variation of moisture and the response of vegetation to varying moisture conditions.

A common approach used in remote sensing to map temporal changes in scene reflectance involves change detection techniques. Change detection techniques discriminate areas of land cover change between two or more dates of imagery using multitemporal data sets. Temporal variations can modify the spectral signatures of features over time thereby changing the grey level value (GLV ranges from 0-255) recorded within a satellite scene. Such changes are most evident for different species of vegetation which are in a continual state of change throughout a growing season. Several researchers (Lam and Hoyt 1972, Deutsch 1976, Anderson *et al.* 1977, Stauffer *et al.* 1978, Adams *et al.* 1980, Byrne *et al.* 1980, Howarth and Wickware 1981, Luce and Turner 1981, Schreier *et al.* 1982, Eyton 1983, Jacobberger 1989, Jacobberger and Hooper 1991, Kumar *et al.* 1993, Gillieson *et al.* 1994, Mishra *et al.* 1994, and Ribed and Lopez 1995) have used change detection techniques on multidate images to determine land cover and land use change. Most importantly, for this study, Jacobberger's (1989)

research on stabilized dunes and desert-fringe environments indicated that spectral features within semiarid to sub-humid zones were controlled mainly by vegetation dynamics as a result of varying moisture conditions. Therefore, the selection of two satellite scenes, one representing a wet period and another representing a dry period, are used in this study to map temporal changes in vegetation.

CHAPTER 2 MULTITEMPORAL PROCESSING

Spectral versus temporal signatures

A spectral signature represents a feature's reflectance pattern as recorded over a series of wavelength bands. Spectral signatures are recorded as grey level values (GLV) in a scale of 0-255 for all bands, visible through the infrared wavelengths. For example, progression from the smaller wavelengths (the visible spectrum) to the longer wavelengths (infrared wavelengths) for vegetation results in a graph of spectral reflectance for specific features (Figure 2.1) called a signature.

One of the most effective ways of displaying the spectral characteristic of surface features is through a false colour image (Dwivedi and Sankar 1992) which evolved from colour infrared aerial photography during World War II. Colour infrared aerial photography uses film that is sensitive to energy in the near infrared, red, and green wavelengths. Since the human eye is only capable of seeing the three primary colours (red, green, and blue), the assignment and interpretation of colours for colour infrared photography is as follows:

1. blue images result from objects reflecting green energy,
2. green images result from objects reflecting red energy, and
3. red images result from objects reflecting near infrared energy.

The success in detecting targets painted green (*i.e.* camouflage) for military purposes, as well as the vivid portrayal of near infrared energy in various tones of red, made false colour infrared photography an important tool in resource analyses prior to the introduction of satellite systems (Lillesand and Kiefer 1994).

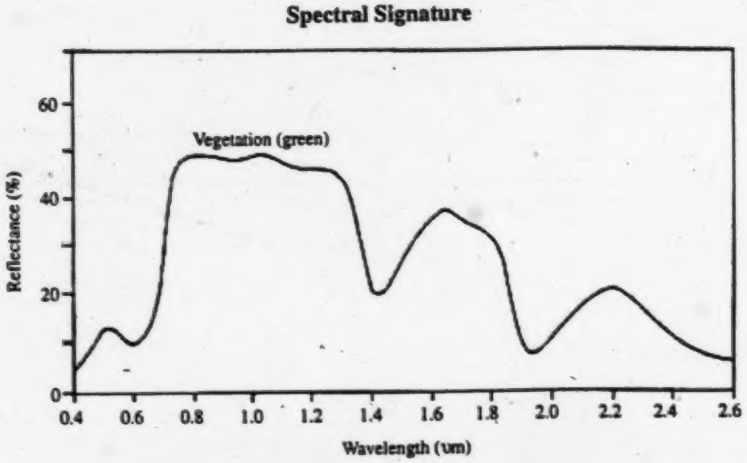

Figure 2.1. Typical spectral reflectance signature for vegetation (after Lillesand and Kiefer, Fig. 1.10 1994).

The first mapping satellite system (Landsat 1) was intended to replicate the colour infrared photographic process. Satellite sensor systems such as the Multispectral Scanner (MSS) and Thematic Mapper (TM) of the Landsat satellites contain four or more spectral bands with at least one band outside the visible spectrum. A Landsat TM false colour composite of the Duchess dune field (Figure 2.2) created by assigning TM4 (infrared 1) to the red gun, TM3 (red) to the green gun, and TM2 (green) to the blue gun, displays moist irrigated, river, and lake vegetation as bright red, the clear lakes as black, the sediment laden river and creek as cyan, drier irrigated areas as yellow, moist grassy vegetation as orange, exposed bedrock, saline areas, and exposed sandy areas along the river as white, and dryland vegetated surfaces as light blue.

Temporal signatures differ from spectral signatures as time not wavelength is used to produce the composite. Multitemporal signatures that model the time behaviour of a feature can be generated by comparing one band of image data over two or more dates. A multitemporal colour composite for each band of image data results in an image where the three primary colours are assigned to three different dates for the same spectral band (Figure 2.3). This composite displays areas of no change, or very little change, in various tones of gray and neutral colours, areas of major reflectance changes as bright colours, and areas of minor changes as subtle colours. For example, Eyton (1983) combined band 5 data for three Landsat MSS dates (May 20 1976, June 25 1976, and August 19 1976) to assess changes in agricultural crops occurring during the growing season.

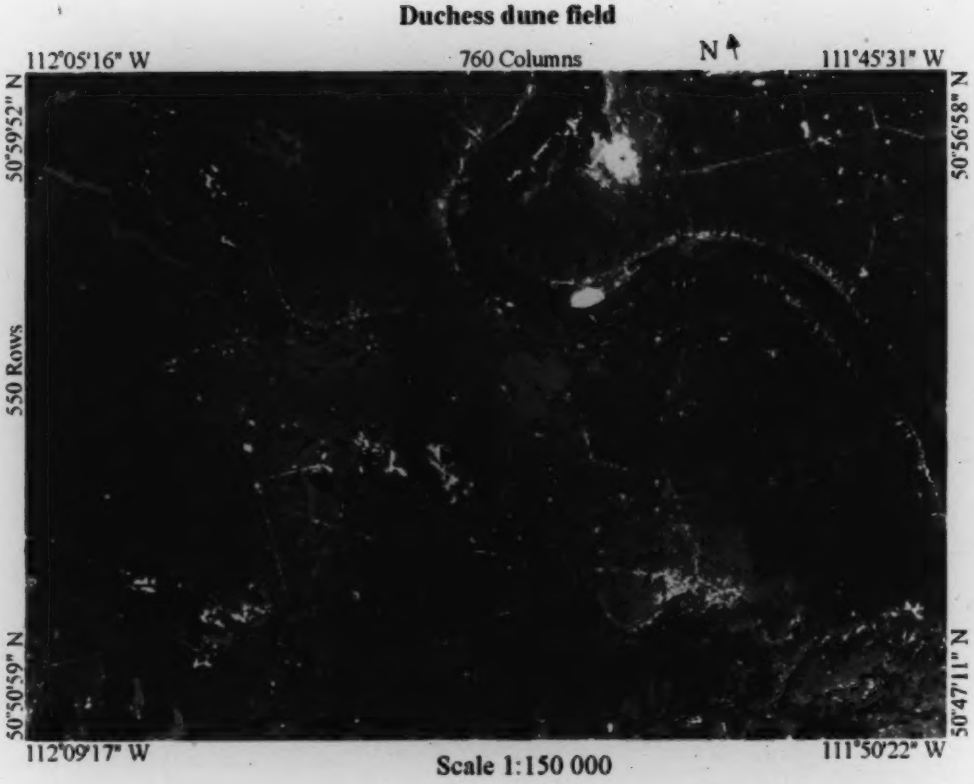

Figure 2.2. False colour composite of the Duchess dune field in southern Alberta. TM4 (infrared 1) was assigned to the red gun, TM3 (red) was assigned to the green gun, and TM2 (green) was assigned to the blue gun.

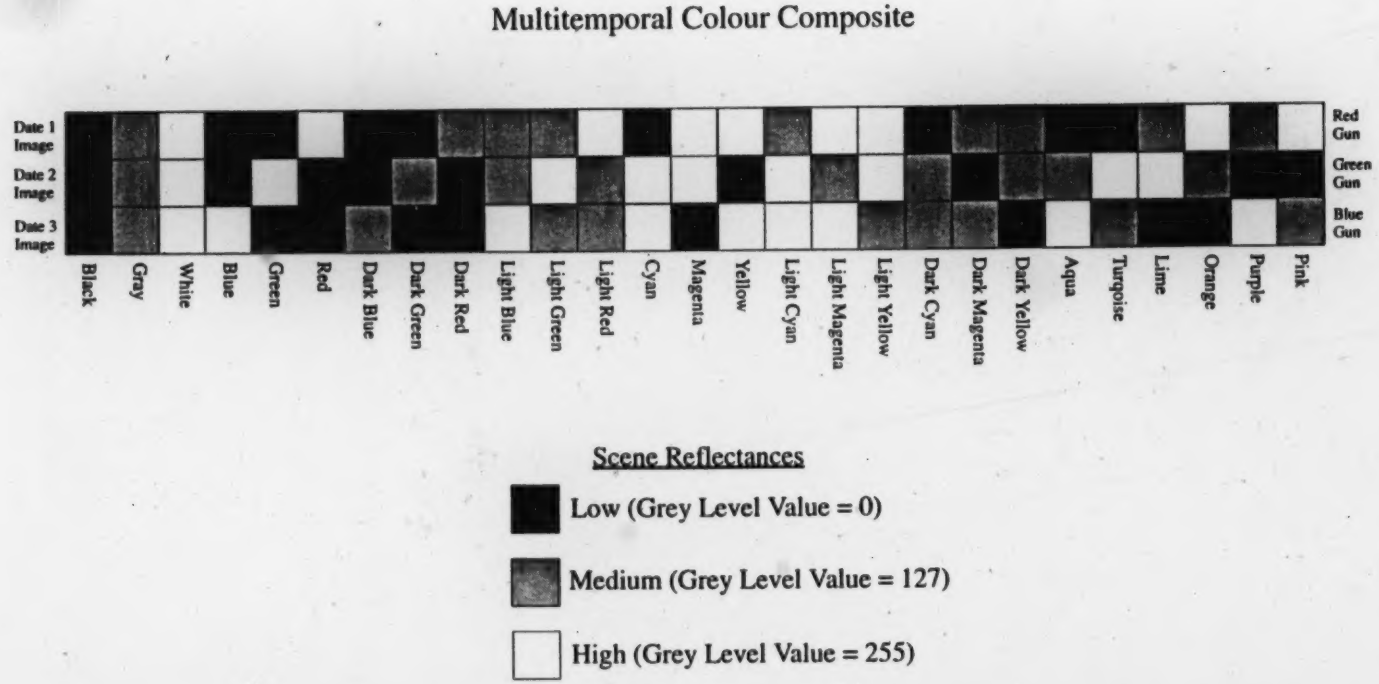

Figure 2.3 . Multitemporal composite colour interpretation key for a 3-date multitemporal image (after Eyton 1983).

The multitemporal composite displayed corn as blue and wheat/beans as orange-yellow which indicated that these crops had changed over the chosen time period. Urban areas appeared as grey tones indicating that no significant change had taken place.

Change detection

Multitemporal data sets are used to discriminate areas of change from areas of no change. The spatial resolutions of the data sets are kept constant and only the date changes. There are four common methods used for change detection; postclassification comparison, multitemporal classification comparison, temporal difference imaging, and temporal difference ratioing (Lillesand and Kiefer 1994). One important image processing technique which is often used in change detection studies is Principal Component Analysis (PCA). The quantity of spectral channels used to create multitemporal images may impede the image interpretation process and in order to decrease the spectral complexity of the data a PCA is often performed (Byrne *et al.* 1980 and Schreier *et al.* 1982). PCA reduces the dimensionality of multi-channel data by producing de-correlated images that retain a maximum amount of significant information within the first two or three principal components (Dwivedi and Sankar 1992). One important disadvantage of using PCA to produce multitemporal images is that temporal differences can occur outside the first three principal components.

Post classification comparison involves independent classification of two or more dates of imagery where visual interpretation of the images allows for the

areas of change to be identified. Howarth and Wickware (1981), Badwar *et al.* (1982), Jacobberger (1989), Jacobberger and Hooper (1991), Kumar *et al.* (1993), and Ribed and Lopez (1995) have used postclassification change detection techniques to determine temporal changes occurring in agricultural areas and arid areas.

Jacobberger (1989) monitored the reflectance characteristics and surface processes in three areas of stabilized dunes (Egypt, Mali, and Botswana) using multitemporal Landsat TM data; an integral component of the research was the effect moisture had on dunes. Three dates for the Egypt, Mali, and Botswana sites were independently classified using supervised training fields. Visual interpretation of the resultant images for each site allowed an assessment to be made of the changes that occurred for all sites. For example, the seasonal differences in sand reflectance during a dry season (March 1986) and a wet season (August 1986) for the Mali site were represented by reflectance in TM4 (infrared 1); TM4 (infrared 1) reflectance decreased during the rainy season and increased during the dry season. The spectral patterns observed from TM4 (infrared 1), in combination with TM3 (red) and TM5 (infrared 2) data, indicated the time of vegetation emergence and simultaneously the time of increased soil moisture for the Mali site. Overall analysis of Landsat TM images for all three sites indicated that surface brightness was controlled by sand composition, while spectral features were controlled by vegetation dynamics.

Multitemporal classification comparison involves simultaneous classification

of two or more dates of imagery. Schreier *et al.* (1982) found that by classifying multitemporal satellite images simultaneously rather than independently an improved contrast is achieved for features that have changed from one date to the next. Schreier *et al.* (1982) used multitemporal classification comparison techniques and Principal Component Analysis (PCA) to define off-road mobility conditions in northern Manitoba based on the presence and distribution of vegetation. Landsat MSS data for three dates (April, May, and June, 1975) was obtained and a PCA was conducted on MSS bands 4,5,6,and 7 for each date. PCA results indicated that within the first two principal components over 97% of the total information content was retained. Analysis of eigenvector loadings for principal components 1 and 2 indicated that bands 5 and 7 were the largest contributors and the final multitemporal classification comparison was conducted using only these bands. Using unsupervised training field selection, three numerically derived clusters were found to be representative of vegetation in the study area. Analysis of colour coded images produced from examination of the cluster analysis results, as well as known ground conditions, led to the production of thematic maps which proved successful in determining off-road mobility.

Temporal image differencing involves the subtraction of GLV of one date from the corresponding GLV of another date. Quantitative measures of temporal change can be assessed using a digital planimeter (Mishra *et al.* 1994) and by calculating threshold values to determine significant amounts of change (Stauffer *et al.* 1978). These methods require recalibration for every temporal set.

Qualitative amounts of change can be assessed by visual interpretation of classed difference images and by superimposing channel specific difference images on top of one another (Gillieson *et al.* 1994). Mishra *et al.* (1994) for example, evaluated environmental degradation in the Aravalli region of the Thar desert in India. Satellite images for 1975, 1984, and 1986 were displayed separately as colour images for visual interpretation of the terrain differences occurring between the dates. Unsupervised training field selection and classification was used to determine the number of classes present for each date and the area for each feature (class) was measured using a digital planimeter. Mishra *et al.* (1994) found that lake areas had decreased by about 66% between 1975 and 1986, that there was an increase of 725% in salinity between 1975 and 1986, and that there was a gradual build-up of aeolian deposits due to shifting sand dunes and sand sheets during this time. Mishra *et al.* (1994) suggested that continual monitoring of the Thar desert using satellite data would provide the basis for determining degradation rates in that area.

Temporal difference ratioing involves the division of GLV from one date from the corresponding GLV of another date. One advantage of temporal ratio comparisons is the decreased variation of scene brightness caused by topography. Normalized Difference Vegetation Indices (NDVI) images are one of the most common difference ratio images produced when the presence of vegetation is a key factor in determining change (Howarth and Wickware 1981 and Jacobberger and Hooper 1991). For example, Jacobberger and Hooper (1991) studied the

geomorphology and reflectance patterns of vegetation-covered dunes at Tsodilo Hills, northwest Botswana, using multitemporal NDVI images. The vegetation density of the dunes was determined using reflectance curves and NDVIs for December 1986, March 1987, June 1987, and August 1987. By independently classifying and interpreting the NDVI images, Jacobberger and Hooper (1991) found that the dune crests showed the strongest seasonal variations in both colour and brightness, while interdune corridors showed a small percentage of seasonal variability.

Classification through time

The time element is critical in achieving optimum contrast between terrain features where spectral changes occur as a result of seasonal and cyclical differences (Schreier *et al.* 1982). For example, in the United States in 1980, nationwide aerial photo coverage during 'leaf-off' and 'leaf-on' conditions was implemented to map land cover during 'leaf-off' conditions and to map vegetation during 'leaf-on' conditions. As vegetation cover types change through time, species differentiation becomes important in accessing change (Lillesand and Kiefer 1994).

Features which exhibit different spectral characteristics through time can be mapped by classifying satellite data for more than one date. Crop classification using remotely sensed data is an established procedure (Li *et al.* 1980). Changes occurring for the same feature as a result of temporal variation would be categorized into separate classes. Deciduous trees for example, would

be categorized into more than one class because seasonal variations in leaf cover cause different spectral response characteristics. Since the needles of evergreen trees essentially remain unchanged during the winter months, a contrast between the evergreen species and the deciduous species is possible.

CHAPTER 3 STUDY SITE AND IMAGE SELECTION

Study site

The Duchess dune field comprises three main areas (Figure 3.1) of aeolian deposits covering a total of approximately 400 km^2. The dunes are mostly of the parabolic type (Figure 3.2) with only a few active blow-out areas (Figure 3.3). The dunes consist of silt to medium-grained sand up to seven metres thick and the interdune areas are predominantly ice-contact lacustrine and fluvial deposits up to twenty-five metres thick (Shetsen 1987). Apart from the dune deposits, the soil found in the Duchess area is a brown chernozem (Kjearsgaard 1983).

The Duchess dune field is in the dry mixed grass ecoregion (Strong and Leggat 1992) of Alberta. The main plant species include needle grasses and blue grama, prairie selaginella, pasture sagewort, moss phlox, and thread-leaved sedge (Strong and Leggat 1992). Wildrose is also common. In areas with more available moisture (usually due to irrigation), buckbrush and silverberry are present. The normal mean annual temperature (1961-1990) of the Duchess area is about 4.0°C and the normal mean precipitation (1961-1990) is about 340.0 mm (Environment Canada 1994). The highest daily mean temperatures and greatest precipitation occur during the summer months (May to September). In winter (December to March), monthly temperatures decrease substantially (by at least 20°C). Based on dune form (parabolic) and dune orientation, Odynsky (1958) indicated that the dune-forming wind was from the northwest, bearing approximately 20 degrees south of east. The approximate date of dune formation

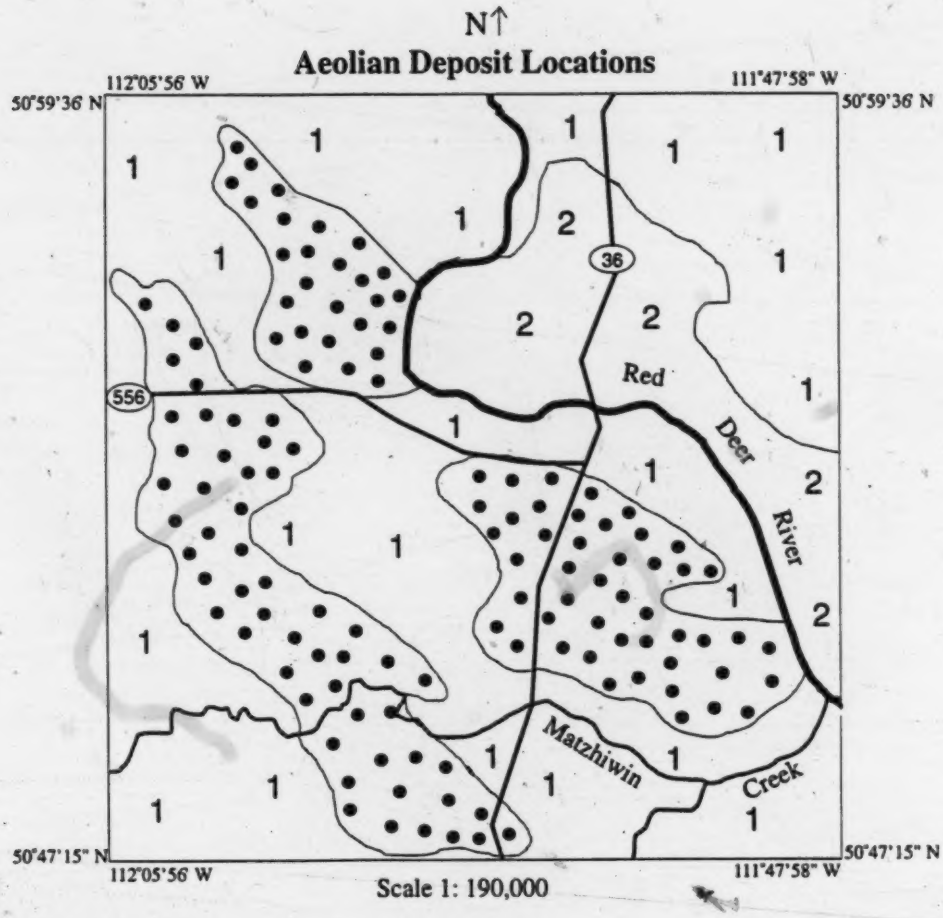

Legend

Aeolian deposit: fine and medium-grained sand and silt: up to 7 m thick; longitudinal and parabolic dunes scoured by blow-outs; undulating to rolling topography.

1 **Ice-contact lacustrine and fluvial deposits, undivided**: gravel, sand, silt and clay, local till; up to 25 m thick; deposited in intermittent supraglacial lakes and streams, or at margins of ice-floored proglacial lakes; undulating to hummocky terrain

2 **Hummocky topography** moderately to weakly developed, with irregularly shaped and poorly defined knobs and kettles; local relief 3 to 10 m.

Figure 3.1. Map of the Duchess dune field showing the relationship of aeolian and other surficial deposits (after Shetsen 1987).

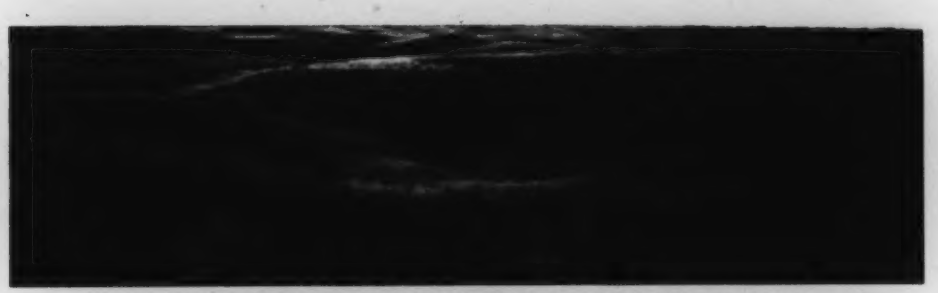

Figure 3.2. Parabolic dunes in the Duchess dune field. Mean crest to trough height variation is approximately 5 m.

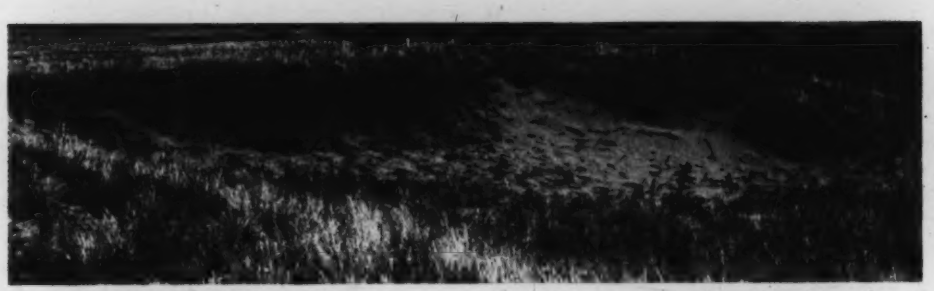

Figure 3.3. Typical small blow-out area (approximately 6 m in length and 2 m in height).

was 12.6 ka B.P. (Bryan *et al.* 1987) based on an estimated date of deglaciation of 13-14 ka B.P. (Dyke and Prest 1987). Wind data collected about 30 km south of the study site, shows that mean monthly wind speeds vary during the year from 12-17 km/hour (Environment Canada 1994).

Image selection

The selection of satellite imagery representing a wet period and a dry period was extremely important in this research as the development of phytogenic dunes is dependent on varying moisture conditions (David 1977). Precipitation data and calculations of the Palmer Drought Index (PDI) for Medicine Hat (Proudfoot 1994) indicated that low precipitation amounts contributed to drought in the prairie provinces throughout the 1980's with the driest year being 1988. The most notable exception was 1986 where departures from mean annual precipitation (1961-1990) showed this was the wettest year within the decade (Figure 3.4). Based on the PDI and departures from mean annual precipitation (from 1961-1990), quick look satellite images (Radarsat International) and path and track information for 1986 and 1988 were used to scan for cloud free coverage during the summers of 1986 and 1988. Analysis of the satellite path and track information (Table 3.1) indicated that the August 07, 1986 satellite scene would be representative of a wet period and the July 20, 1988 scene would be representative of a dry period as cloud free coverage was available on these dates. The digital image data used in this study was acquired by the Landsat 5 Thematic Mapper (TM) sensor. The footprint of the registered Landsat TM scene

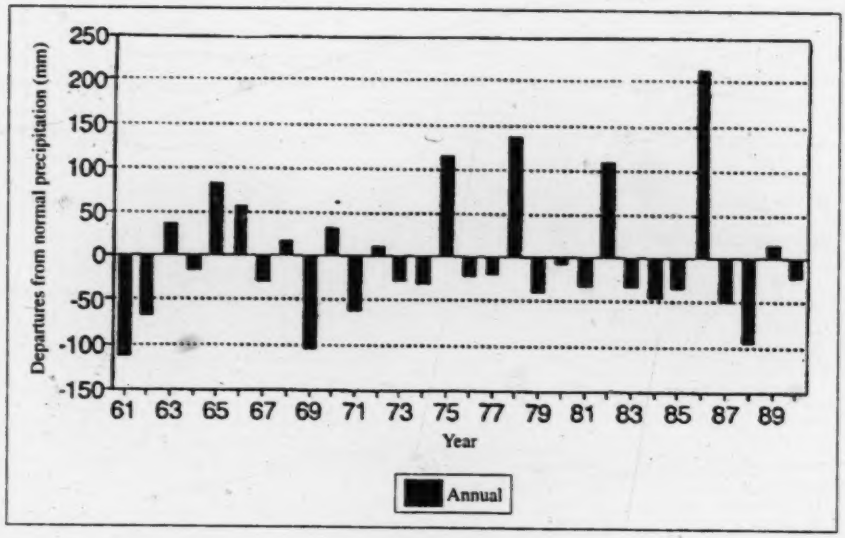

Figure 3.4. Departures from 1961-1990 mean annual precipitation (mm) for Medicine Hat (Proudfoot 1994).

Table 3.1. Path and Track Information for the Wet Period and the Dry Period Satellite Data.

	Wet Year	*Dry Year*
Acquistion Date	August 07, 1986	July 20, 1988
Rows	1024	1024
Columns	1024	1024
Pixel Size	30 metres 120 metres (TM6)	30 metres 120 metres (TM6)
Sun Elevation (degrees)	40	43
Solar Azimuth (degrees)	62	60
Centre	50°59'58" N 111°27'14" W	50°44'18"N 111°26'24" W
Satellite	Landsat-5	Landsat-5
Instrument	Thematic Mapper	Thematic Mapper
Cloud Cover	0%	0%

(Figure 3.5) covers an area 16.5 km by 22.8 km. Seven channels of Landsat TM data (red, green, blue, infrared 1, infrared 2, thermal, and infrared 3) were acquired each with a spatial resolution of 30 m except for the thermal band (TM6) which has a spatial resolution of 120 m. TM6 was not used for mapping because the resolution was too coarse and the value of daytime thermal emissions is minimal due partly to topographic effects.

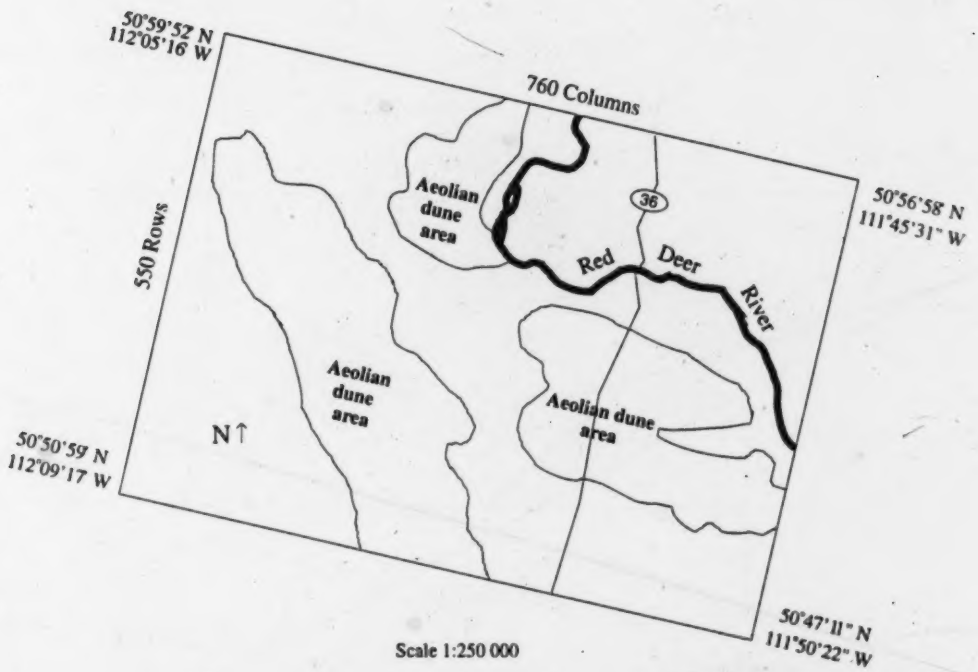

Figure 3.5. Registered Landsat TM footprint showing main areas of the Duchess dune field.

CHAPTER 4

MULTITEMPORAL IMAGE PROCESSING AND INTERPRETATION

Image registration

Prior to the processing of multidate imagery, accurate spatial registration of the imagery is required for effective change detection. Registration procedures involve identification of ground control points, development of registration equations based on the control points, and 'rubber sheeting' of one data set to the other using resampling (Wolf 1974). After corresponding ground control points are located for each date of imagery an equation is derived which finds the mathematical relationship between each image date. If one data set is 'a' and the other is 'b' (where 'a' is a function of 'b') the following functions apply:

$$\text{Row}_a = f(\text{Row}_b, \text{Column}_b)$$
$$\text{Column}_a = f(\text{Row}_b, \text{Column}_b)$$

After the coefficients in the above functions are solved, the co-ordinate system of 'a' is rubber sheeted to a blank data set that has the same coordinate system as 'b'. All pixels in 'a' are resampled to match the co-ordinate location of all pixels in 'b'. There are three approaches for resampling; nearest neighbour, bilinear, and cubic convolution. Of these approaches, nearest neighbour maintains the radiometric integrity in GLV of 'a' when it is resampled to correspond to the coordinate locations of 'b'. The other two approaches may produce smoother and sharper looking images but radiometric integrity is not retained.

The original miniscenes (1024 rows X 1024 columns) received from Radarsat International were subsetted to eliminate coverage not pertinent for this

research. The subsets were generated using the program SUBCON in TERRA FIRMA (Eyton 1992) to cover only the Duchess dune field and resulted in an image of 550 rows by 760 columns. To locate the minimum and maximum UTM coordinates for the registered image, two 1:50 000 NTS topographic map sheets (72L 13 and 82I 16) were used. A control point file was then generated using on-screen digitizing of six control points from the wet data set. The same six corresponding control points were then digitized from the dry data set. TM bands 1-5, and 7 of the dry data set were registered to TM bands 1-5, and 7 of the wet data set using the IDRISI (Eastman 1993) program RESAMPLE. The IDRISI program is a two step registration program. The first step involves solving for coefficients (based on ground control points) and the second step involves resampling.

Principal Components Analysis (PCA)

PCA is a data transformation technique that provides a systematic means of reducing the dimensionality of the multi-band TM data (Dwividi and Sankar 1992 and Lillesand and Kiefer 1994). PCA separates non-random variance (information content) from most random variance (noise) by containing the information content within the first two or three principal components. A PCA was performed on a total of twelve raw bands (six for the wet data set and six for the dry data) using the program PCOMP in TERRA FIRMA. Twelve raw principal component images resulted. To improve the feature distinction within each image, contrast stretching was performed. Using COUNT in TERRA

FIRMA clipping values (2.5% for each tail) for each black and white principal component image were determined. Using the program GRAY in TERRA FIRMA each principal component image was independently rescaled according to its corresponding grey level clipping values. After the twelve principal component images were contrast stretched, each image was sharpened (10 or 20%) in PICLAB (Crocker 1990) to enhance the edges.

Multitemporal eigen images and composites

Normally the first three principal components are used to create a principal component colour composite because they explain the majority of system variance (Schreier *et al.* 1982). This is often reconfirmed by eigenvalues that are greater than one. In this analysis, the first three principal components accounted for 85.61% of the total variance (Table 4.1) and not until principal component 6 was over 98% of the variance explained. Also the eigenvalues for principal components 1 and 2 are greater than one but all other eigenvalues are less than one. Further analysis of each principal component was conducted by analyzing the eigenvector values or loadings (Table 4.2). To interpret eigenvector loadings the sign designation (negative or positive) and numerical value of the loadings are examined. For example, in principal component 1 all bands have similar loadings with the exception of TM4 (infrared 1) which has a lower loading for both the wet and the dry year. Since there are no positive or negative differences between the wet and the dry data set in addition to similar band loadings, principal component 1 is a brightness image with no temporal differences. Principal component 2

Table 4.1. Eigenvalue Report for the 12 Principal Components Generated From Raw Data for the Wet and the Dry Year.

	Eigenvalue	Proportion of Variance	Explained Variance
PC 1	7.5429	0.6286	0.6286
PC 2	1.8326	0.1527	0.7813
PC 3	0.8973	0.0748	0.8561
PC 4	0.7058	0.0588	0.9149
PC 5	0.5181	0.0432	0.9581
PC 6	0.2702	0.0225	0.9806
PC 7	0.0890	0.0074	0.9880
PC 8	0.0511	0.0043	0.9922
PC 9	0.0369	0.0031	0.9953
PC10	0.0278	0.0023	0.9976
PC11	0.0176	0.0015	0.9991
PC12	0.0108	0.0009	1

Table 4.2. Eigenvector Loadings for the 12 Principal Components Generated From Raw Data for the Wet Year and the Dry Year.

Band No.	PC 1	PC 2	PC 3	PC 4	PC 5	PC 6
1	0.333	-0.0886	-0.2317	-0.2339	-0.2382	-0.0265
2	0.3333	-0.043	-0.2599	-0.244	-0.2547	-0.0394
3	0.3421	-0.0781	-0.1387	-0.2389	-0.2409	0.085
4	0.0158	0.6799	-0.1124	-0.0707	-0.0366	-0.7061
5	0.3142	0.1824	0.3932	-0.1049	-0.1759	0.0352
6	0.3366	0.0574	0.278	-0.1367	-0.1983	0.1453
7	0.3122	-0.0843	-0.3676	0.3578	0.162	-0.0774
8	0.3034	-0.0539	-0.4131	0.3855	0.1791	-0.0132
9	0.2426	-0.1159	0.0804	-0.5226	0.7975	-0.1084
10	-0.0021	0.6622	-0.2495	-0.0681	0.1705	0.6705
11	0.3064	-0.1504	0.3938	0.3355	0.1143	0.0338
12	0.3261	0.0284	0.2922	0.3565	0.1107	-0.032

Band No.	PC 7	PC 8	PC 9	PC10	PC11	PC12
1	0.3412	-0.4749	-0.1912	0.5796	-0.0308	-0.0064
2	0.2551	0.2597	0.2598	-0.3902	-0.5816	-0.055
3	0.0638	0.2754	0.0605	-0.206	0.7805	-0.0062
4	-0.0166	0.0702	-0.074	0.0216	0.0736	0.0579
5	-0.4407	-0.3621	0.3781	-0.0269	-0.0161	-0.4484
6	-0.4338	0.2309	-0.4601	0.0841	-0.1956	0.478
7	-0.1967	-0.4655	-0.3078	-0.4967	0.0307	0.0472
8	-0.3358	0.3159	0.3631	0.4559	-0.0288	0.0218
9	-0.0088	0.0093	0.0091	0.0022	-0.0083	0.0032
10	0.0826	-0.0187	-0.0629	-0.0104	-0.017	-0.0671
11	0.4233	-0.1477	0.3637	-0.0528	0.0645	0.5114
12	0.3072	0.3212	-0.4114	0.0603	-0.0364	-0.5434

Band Numbers

1=TM1 (blue) of the dry data set
2=TM2 (green) of the dry data set
3=TM3 (red) of the dry data set
4=TM4 (infrared 1) of the dry data set
5=TM5 (infrared 2) of the dry data set
6=TM7 (infrared 3) of the dry data set
7=TM1 (blue) of the wet data set
8=TM2 (green) of the wet data set
9=TM3 (red) of the wet data set
10=TM4 (infrared 1) of the wet data set
11=TM5 (infrared 2) of the wet data set
12=TM7 (infrared 3) of the wet data set

differs from principal component 1 because most of the information content comes from TM4 (infrared 1) in the wet and the dry year. Since TM4 (infrared 1) is useful in determining vegetation types, vigour, biomass content and soil moisture discrimination (Lillesand and Kiefer 1994), principal component 2 is representative of vegetation dynamics with no temporal discrimination. Temporal contrast is shown by the eigenvector values of principal components 4, 5, 6, 7, 10, 11, and 12 because in most cases the signs (positive or negative) are reversed when comparing the wet year to the dry year. Principal component 5 is a good example of this as all the loadings for the dry year are positive whereas all the loadings for the wet year are negative. This indicates a direct contrast or difference between the wet and the dry year. Also of interest is principal component 4 which receives the highest loading from TM3 (red) in the wet year and principal component 6 which receives the highest loading from TM4 (infrared 1) in the dry year. The loadings for principal components 4 and 6 represent a change in the vegetation during the wet year possibly as a result of increased moisture conditions. All other principal components were interpreted in this manner and the interpretations are presented in Table 4.3.

Interpretation

The loadings for each principal component can be explained in terms of their information content and it is possible to define four rough principal component or eigen image groupings. Colour composites (Figures 4.1 to 4.4) were generated using the program COMP in TERRA FIRMA following the

Table 4.3. Principal Component Analysis Interpretation of the 12 Principal Components Generated for Raw Data for the Wet Year and the Dry Year.

Principal Component Band	Interpretation
Principal component 1	Represents a brightness image for both the wet and the dry year with the exception of TM4 (infrared 1).
Principal component 2	Represents vegetation dynamics seen in TM4 (infrared 1) only for both the wet and the dry year.
Principal component 3	Represents the short wavelengths versus the long wavelengths with no regard to temporal variations.
Principal component 4	Represents temporal contrast for TM1 (blue), TM2 (green), TM5 (infrared 2), and TM7 (infrared 3) over time with no difference shown in TM4 (infrared 1). Note, the vegetation's response in TM3 which is loaded negatively in both the wet and the dry year with emphasis during the wet year.
Principal component 5	Represents a temporal contrast for all bands, with emphasis on the difference that occurs in TM3 (red) during the wet year.
Principal component 6	Represents a contrast between the wet and the dry year for TM4 (infrared 1) only.
Principal component 7	Represents a contrast between the wet year and the dry year for TM1 (blue), TM2 (green), TM5 (infrared 2), and TM7 (infrared 3).
Principal component 8	Represents the shortest two wavelengths (TM1-blue and TM2-red) versus longest two wavelengths (TM5-infrared 2 and TM7-infrared 3) with no regard to temporal variation.
Principal component 9	Represents the shortest two wavelengths versus the longest two wavelengths with no regard to temporal variation..
Principal component 10	Represents a temporal difference in TM1 (blue) and TM2 (green).
Principal component 11	Represents a small temporal contrast between TM2 (green) and TM3 (red) for the wet year and for the dry year.
Principal component 12	Represents a small temporal contrast between TM5 (infrared 2) band and TM7 (infrared 3) for the wet and for the dry year.

**Note, small temporal differences occur where the explained variation of the principal component is less than 1%.

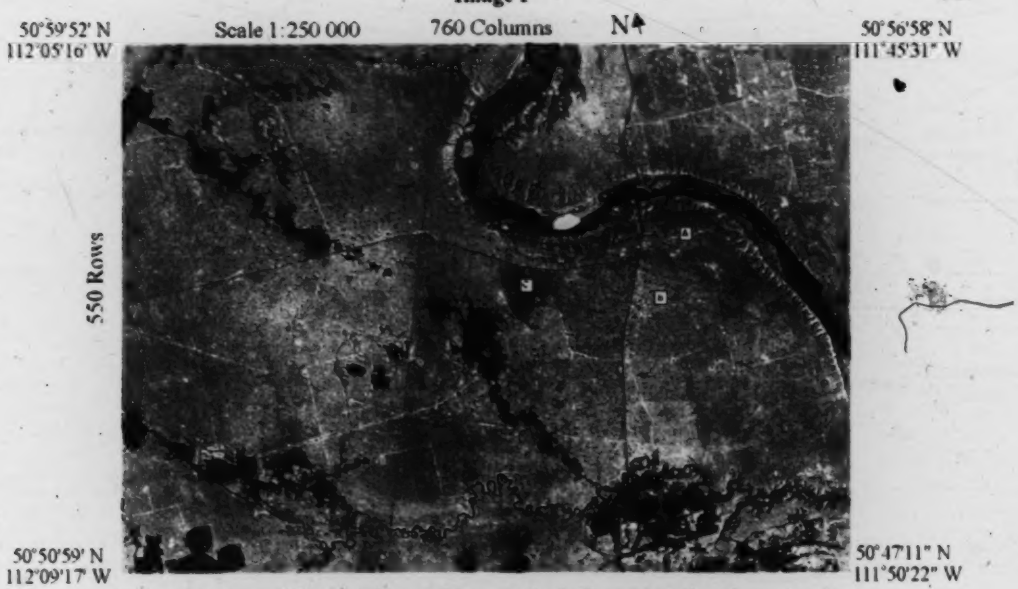

Figure 4.1. Image I is a brightness PC image including vegetation dynamics that was generated by assigning PC1 to the red gun, PC2 to the green gun, and PC3 to the blue gun. Area 'A' represents dune-free prairie grassland, area 'B' represents aeolian dune deposits, and area 'C' represents irrigated areas.

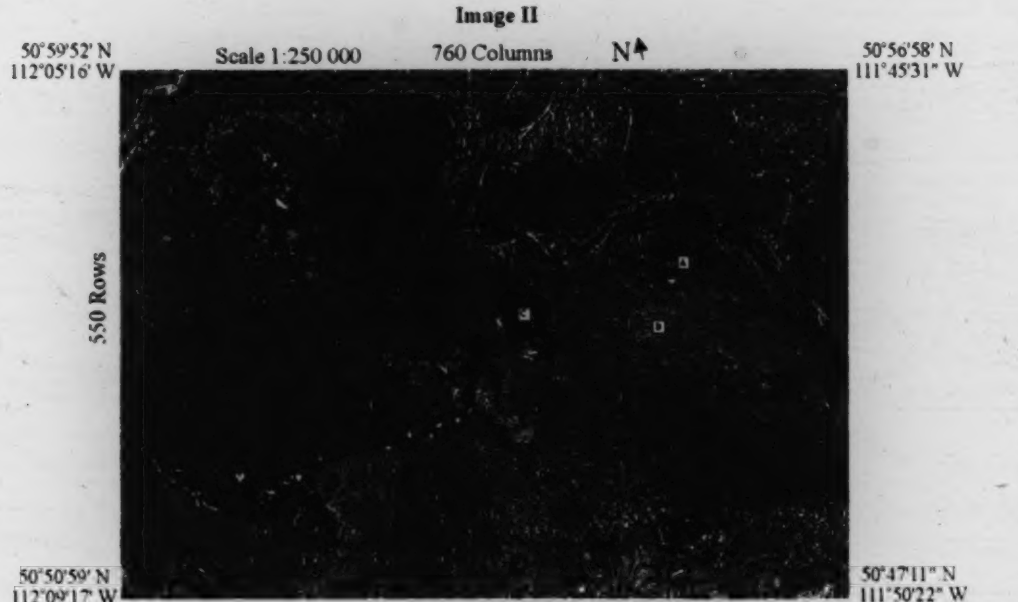

Figure 4.2. Image II is a temporal PC image generated by assigning PC4 to the red gun, PC5 to the green gun, and PC6 to the blue gun. See Figure 4.1 for explanation of area 'A', 'B', and 'C'.

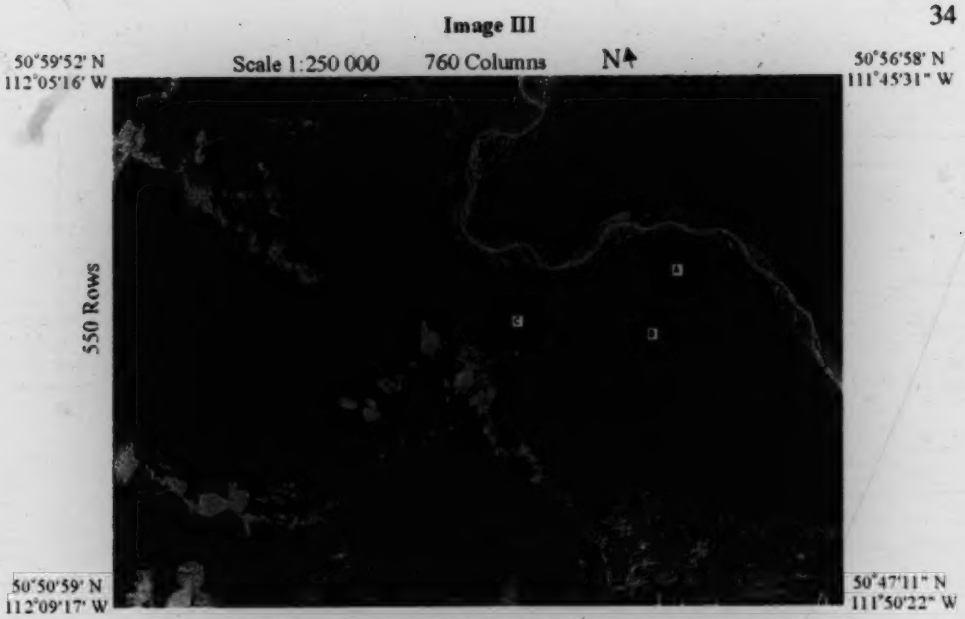

Figure 4.3. Image III is a temporal PC image for the visible and the infrared bands generated by assigning PC 7 to the red gun, PC8 to the green gun, and PC9 to the blue gun. See Figure 4.1 for explanation of areas 'A' - 'C'.

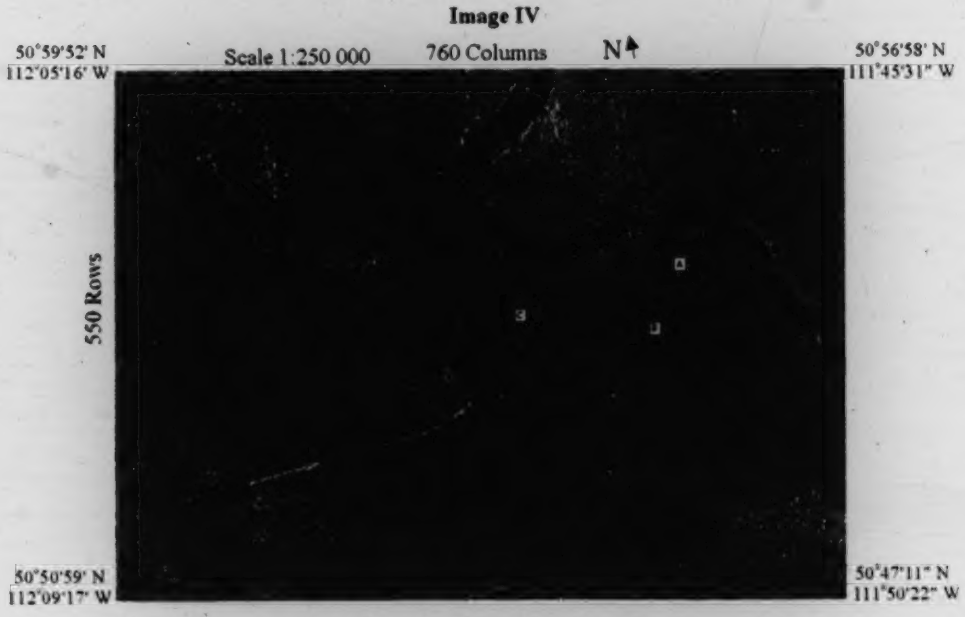

Figure 4.4. Image IV is a temporal PC image showing small temporal contrasts generated by assigning PC10 to the red gun, PC11 to the green gun, and PC12 to the blue gun. See Figure 4.1 for explanation of areas 'A' 'B', and 'C'.

grouping shown in Table 4.4. Assignment of principal component 1 to the red gun, principal component 2 to the green gun, and principal component 3 to the blue gun results in an image (Figure 4.1) with no temporal contrast. The colour variation in this composite is minimal consisting of magenta, yellow, dark green, and light green colours. The darker green areas around the lakes, river, and creek and the lighter green areas on the sand dunes occur because principal component 2, which is the band representing vegetation dynamics, is assigned to the green gun. When red and blue are subtractively mixed magenta results and this means that this composite receives most of its information content from principal components 1 and 3. Yellow areas represent areas of zero to minimal vegetation cover (*e.g.* blow-out dunes, exposed bedrock, and saline areas). Dune areas can be identified approximately based on the vegetation displayed as light green (area 'A') yet this composite is not sufficient in determining aeolian from non-aeolian boundaries. Other features such as roads, the Red Deer River, creeks, and irrigated areas (area 'C') are well defined due to the visible spectrum component within the image. Variation from light to dark green in the irrigated areas occurs because light green represents drier vegetation and dark green represents moist vegetation.

Assignment of principal components 4, 5, and 6 to the red, green, and blue guns respectively produces an image (Figure 4.2) where strong temporal differences can be seen in many locales (areas 'A', 'B', and 'C' in Figure 4.2). Compared to Figure 4.1, this image is not only more colourful but is much more

Table 4.4. Four Colour Composite Eigen Images Generated Using Principal Component Analysis.

Total information content (%)	Eigen Image	Principal Components	Eigen Image Interpretation
85.61	1	PC 1 PC 2 PC 3	Brightness image with vegetation dynamics
12.45	2	PC 4 PC 5 PC 6	Temporal difference image
1.47	3	PC 7 PC 8 PC 9	Specific Visible and IR temporal difference image
0.47	4	PC10 PC11 PC12	Spectral difference image where contrast is small (eigenvalue is small).

effective in distinguishing aeolian from non-aeolian material. For example, area 'A' on Figure 4.2 appears dull grey because of vegetation growth in the wet year and vegetation desiccation in the dry year. This same area in Figure 4.1 appears magenta as only the brightness elements are being displayed. In area 'B' (Figure 4.2) dune boundaries are apparent due to changes in the vegetation cover as a result of moisture fluctuations. The temporal aspect of principal components 4, 5, and 6 cause these colour variations to occur. This same area ('B') on Figure 4.1 has very little colour variation as some of the vegetation on the dunes is light green and the rest of the vegetation is magenta. The irrigated areas (see area 'C' in Figure 4.2) also illustrate temporal variations through colour variation. For example, blue, purple, and cyan represent irrigated areas in Figure 4.2 yet these same areas appear light to dark green or do not exist in Figure 4.1. Although Figure 4.2 represents only 12.45% of the total information content, the temporal aspect of the principal components is effective in distinguishing aeolian from non-aeolian material. Interestingly, Figure 4.2 also displays dune morphology. For example, in area 'B' the characteristic U-shaped form of parabolic dunes is apparent.

Assignment of principal components 7, 8, and 9 to the red, green, and blue guns respectively produces an image (Figure 4.3) that is not very effective in defining boundaries between aeolian and non-aeolian material. The main colour in this composite is purple which results with varying combinations of red, green, and blue. Purple indicates that all principal components (7, 8, and 9) used in this

eigen image are displayed. The yellow (a mixture of red and green) seen in the moist areas such as the Red Deer River, lakes, creeks, and irrigated areas results because PC9 has low reflectance for these features and principal components 7 and 8 have high reflectance for these features. Principal component 7 is the only principal component that contains temporal contrast between the wet period and the dry period. Figure 4.3, representing 1.47% of the total information content, shows the vegetation differences occurring in the irrigated areas but is not effective at delineating the sand dune areas.

The final composite comprising principal components 10, 11, and 12 (Figure 4.4) is more effective in showing temporal contrast or difference than the composite comprising principal components 7, 8, and 9 because all three principal components contain temporal contrast information. Although this image is washed out in appearance, differences in the vegetation associated with the river and the irrigated areas (*i.e.* wet and moist) show up quite well. In the sand dune areas there appears to be some variation in colour which is indicative of the vegetation's response to wet versus dry conditions. The boundaries, however, are not well defined due to the low information content of this image (0.47%). Overall, the washed out effect of this composite makes interpretation difficult.

All the eigen image composites (Figures 4.1 to 4.4) contain different information that may be useful for mapping aeolian sand deposits. Of the four composites produced, Figure 4.2 appears to be the most useful in delineating the sand dunes and the dune field boundaries from other surrounding features. This

occurs because dune trough vegetation, which normally prefers lower topography and higher moisture availability, advances onto the drier dune crest locations because of increased moisture. As areas of change are being identified, the dune morphology becomes more apparent as topography is an important factor in the location of vegetation species.

Of all the principal components, temporal differences are represented by principal components 4, 5, 6, 7, 10, 11, and 12. The generation of a colour composite using all these principal components is not possible as assignment of only one principal component image to the red gun, to the green gun, and to the blue gun is possible. The generation of another PCA on only these principal components would not be feasible as further complexity would occur making interpretation of these images difficult.

One other PCA approach would be to create an image assigning principal component 5 to the red gun, principal component 2 to the green gun, and principal component 6 to the blue gun. Analysis of the eigenvector values for these principal components suggest that an image showing temporal differences and vegetation dynamics should result. A principal component colour image combining information for principal components 2, 4, and 5 was created but this image was not as effective at determining dune boundaries or dune shape as the principal component colour image produced using principal components 4, 5, and 6.

PCA showed that the use of temporal data is extremely valuable when

mapping dune areas and that temporal differences between the wet and the dry periods were found in principal components containing less than 10% of the total information content. In order to include all data in the analysis (including both temporal differences and spectral differences) on one image, unsupervised training field selection and classification was used. Training field selection (supervised or unsupervised) and classification procedures can classify image data from several bands and several dates simultaneously. This allows for areas of change from time 1 to time 2 to be identified and can aid in defining boundaries between different surface features.

CHAPTER 5

MULTITEMPORAL IMAGE CLASSIFICATION AND ANALYSIS

Classification

To categorize all pixels in an image into land cover classes or themes an analyst must first select training fields, and second must assign a class number or theme to every pixel in the image. There are two basic approaches for selecting training fields; supervised or unsupervised. In supervised training field selection the image analyst identifies the types of features in a scene based on prior knowledge of the area and develops categories based on the training areas selected. The unsupervised training field selection approach differs from the supervised training field selection approach as pixels in an image are categorized into natural spectral groupings or clusters using sampling procedures such as cluster analysis. The unsupervised training field selection approach is most often used when the analyst has no prior knowledge of the area.

In this research unsupervised training field selection was used, and, in so doing, a cluster analysis was performed. Cluster analysis is a sampling procedure where the sampling number (*i.e.* every 10th pixel) is determined by the analyst (Johnston 1978). Cluster analysis techniques use Analysis of Variance to group sample observations that are similar (achieved when minimum within group variance is reached) and simultaneously to separate sample observations that are dissimilar (achieved when maximum between-group variance is reached). The group number at which the minimum within-group variance and the maximum

between-group variance first occurs will produce a large F-Ratio (division of within-group variance by between-group variance). This F-ratio when plotted acts as a guide to assist the analyst in determining the appropriate number of groups to represent the data. Each observation that has been sampled using cluster analysis techniques is then designated a cluster number to which that observation belongs.

In order to develop a classification from cluster analysis results, a classifier is built which determines the decision rules that breaks up data space into feature space. There are several classifiers which are based on different 'decision-rule' geometry. For example, a parallelepiped classifier produces 'box-like' feature spaces; discriminant analysis classifiers produce feature spaces that are defined by straight lines that are not necessarily parallel to the data space axes; and maximum likelihood classifiers can be described as set of equiprobability ellipses (Figure 5.1). Of these classifiers the discriminant analysis classifier forces every pixel within the data set to be assigned a class, whereas, the other two classifiers may leave pixels labelled as 'unknown' due to the pixel distance away from the box centre or equiprobability ellipse centre.

In this research discriminant analysis was used to classify the satellite data; this leaves no unclassified data. Discriminate analysis involves the assignment of a class number to every pixel based on the calculation of discriminant functions. Discriminant functions are built from the cluster analysis data by computing discriminant function scores for each group or cluster. Each discriminant function

Parallelepiped Classifier

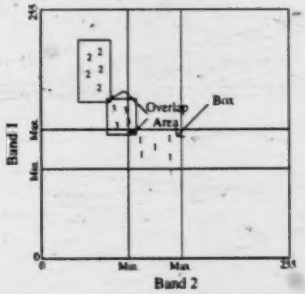

In the parallelepiped classifier a box displaying similar pixels is formed if:

1. The grey level value (GLV) of Band 1>Band 1 min. and the GLV of Band 1<Band 1 max.
2. The glv of Band 2 >Band 2 min. and the GLV of Band 2<Band 2 max.

Discriminant Analysis Classifier

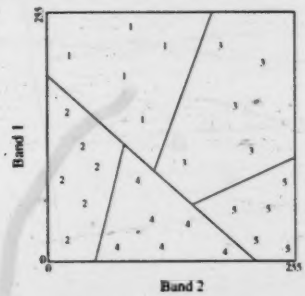

The discriminant analysis classifier creates a territorial plot of the image data by forcing every pixel into a category or class.

Maximum Likelihood Classifier

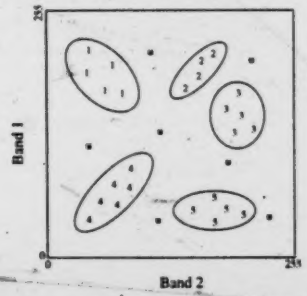

In the maximum likelihood classifier equiprobability ellipses are used to determine categories and classes for the image data. If a pixel does not fall within an ellipse the pixel is left as unknown (u).

Figure 5.1. Three types of classifiers used in the classification of image data.

score within a group is averaged to compute the mean score or the group centroid. Discriminant functions which are represented by vectors, divide up the data space into feature space. Each pixel is assigned a class number based on each pixel's discriminant function score.

Multitemporal classification

The unsupervised training field selection approach used for this research required that all twelve data files (six for the wet and six for the dry) be input into the program TRAIN in TERRA FIRMA. An unsupervised k-means cluster analysis was conducted by sampling every fifteenth row and fifteenth column and by allowing up to 20 classes to be created. From an F-ratio graph (Figure 5.2) the number of 'optimal' clusters was determined to be 15 as this is where there the first sharp peak (local maxima) in the data occurs. A small peak occurs at cluster 10 yet the F-ratio at cluster 15 is greater thereby making 15 the 'optimal' number of clusters. TRAIN was then run again on all twelve data sets to assign each observation for all data sets to a cluster number between 1 and 15.

Next a Fisher's discriminant analysis classifier was used where each pixel of the data sets (twelve bands of data) was forced into one of 15 classes. Cluster analysis results were used as input in the program CLASS in TERRA FIRMA which calculates discriminate functions. The resultant image file made up of fifteen classes or themes was modally filtered to remove the unwanted 'salt and pepper' effect of the single classed pixels surrounded by pixels of another class. Fifteen theme maps (Figures 5.3 to 5.17) and 15 corresponding multitemporal

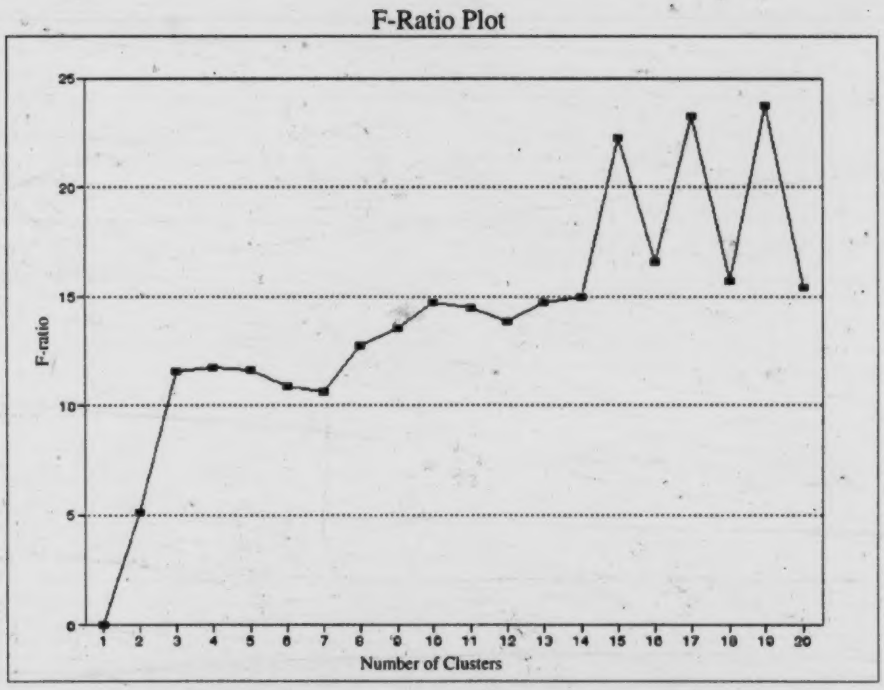

Figure 5.2. F-ratio plot generated using cluster analysis combining Thematic Mapper data for both the wet year and the dry year.

Class 1

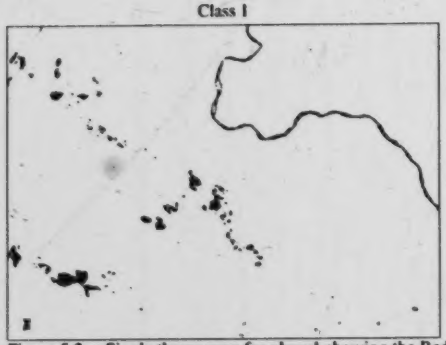

Figure 5.3a. Single theme map for class 1 showing the Red Deer river and lakes.

Class 2

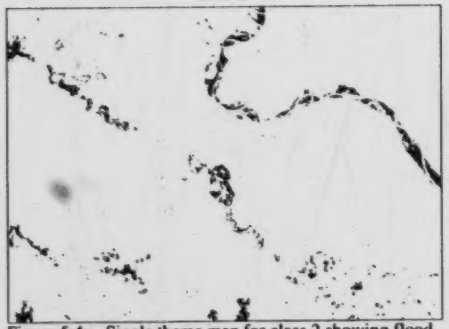

Figure 5.4a. Single theme map for class 2 showing flood-plain vegetation.

Class 3

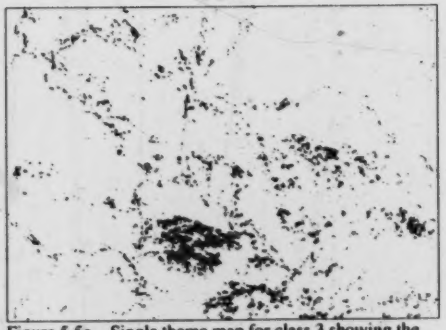

Figure 5.5a. Single theme map for class 3 showing the aeolian dunes associated with dune crest vegetation.

Class 1

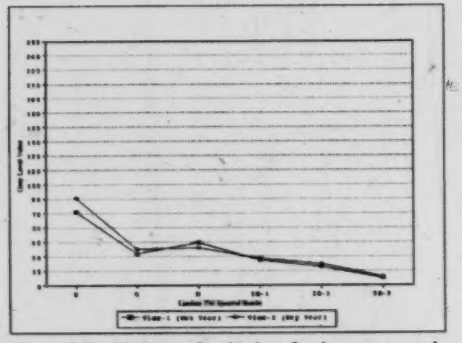

Figure 5.3b. Mean grey level values for the wet year and the dry year for raw data comprising class 1.

Class 2

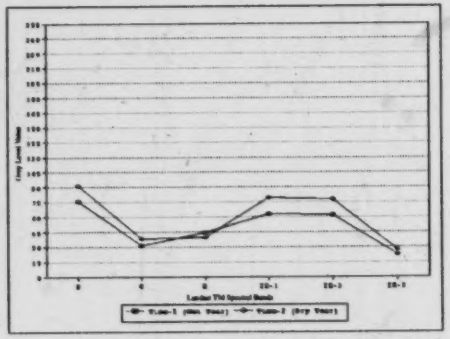

Figure 5.4b. Mean grey level values for the wet year and the dry year for raw data comprising class 2.

Class 3

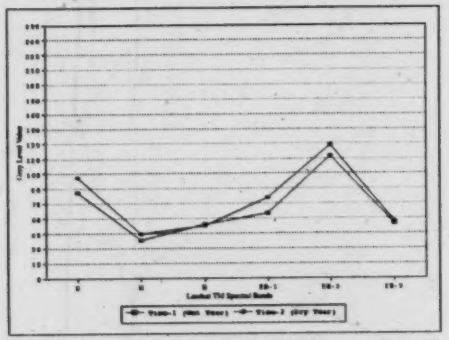

Figure 5.5b. Mean grey level values for the wet year and the dry year for raw data comprising class 3.

Class 4

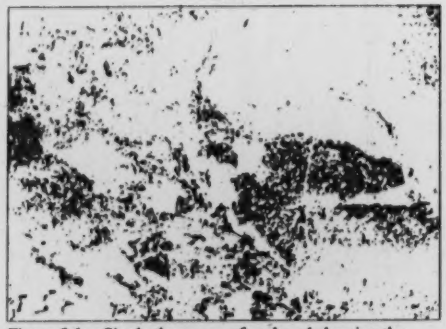

Figure 5.6a. Single theme map for class 4 showing the aeolian dunes associated with dune trough vegetation.

Class 5

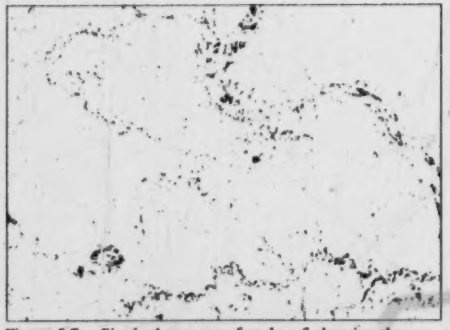

Figure 5.7a. Single theme map for class 5 showing the vegetation associated with the Red Deer River and lakes.

Class 6

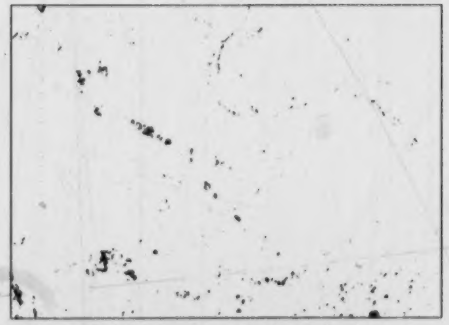

Figure 5.8a. Single theme map for class 6 showing vegetation associated with sloping terrain near the Red Deer River and lakes.

Class 4

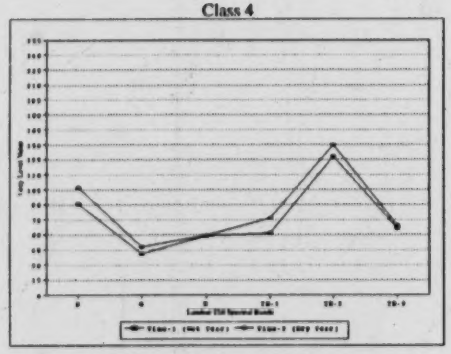

Figure 5.6b. Mean grey level values for the wet year and the dry year for raw data comprising class 4.

Class 5

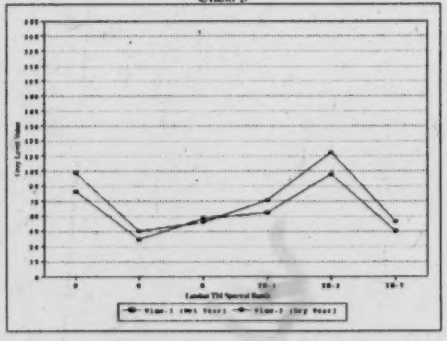

Figure 5.7b. Mean grey level values for the wet year and the dry year for raw data comprising class 5.

Class 6

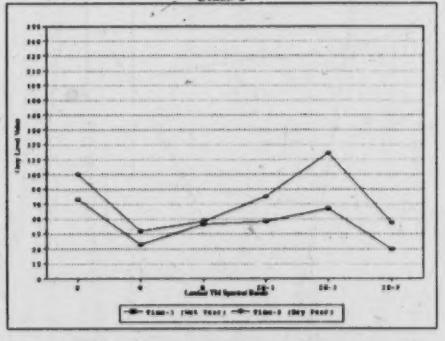

Figure 5.8b. Mean grey level values for the wet year and the dry year for raw data comprising class 6.

Class 7

Figure 5.9a. Single theme map for class 7 showing the vegetation associated with valley sides of the Red Deer River and lakes.

Class 8

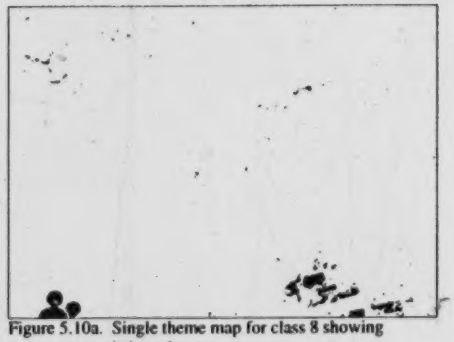

Figure 5.10a. Single theme map for class 8 showing irrigated areas.

Class 9

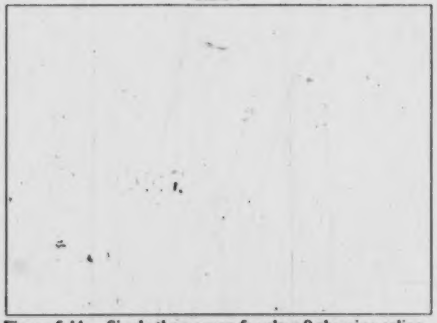

Figure 5.11a. Single theme map for class 9 showing saline deposits associated with lakes.

Class 7

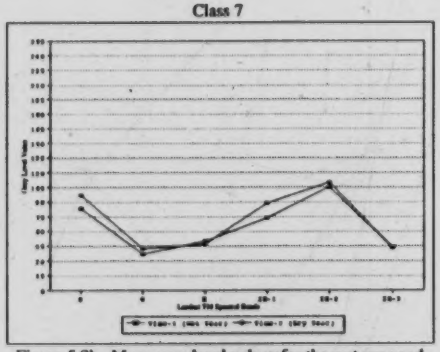

Figure 5.9b. Mean grey level values for the wet year and the dry year for raw data comprising class 7.

Class 8

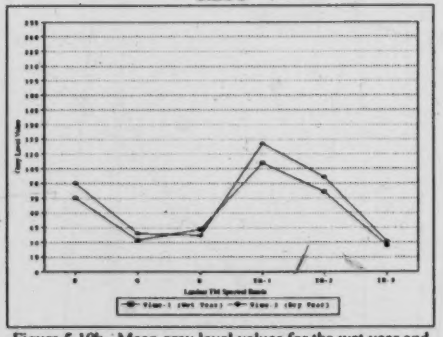

Figure 5.10b. Mean grey level values for the wet year and the dry year for raw data comprising class 8.

Class 9

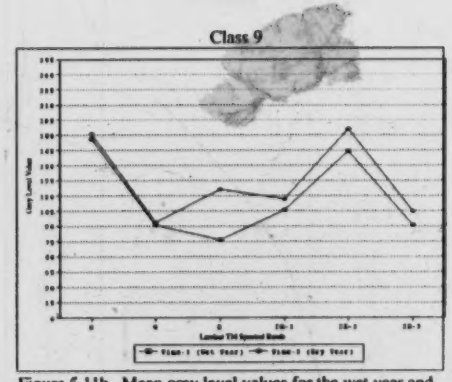

Figure 5.11b. Mean grey level values for the wet year and the dry year for raw data comprising class 9.

Class 10

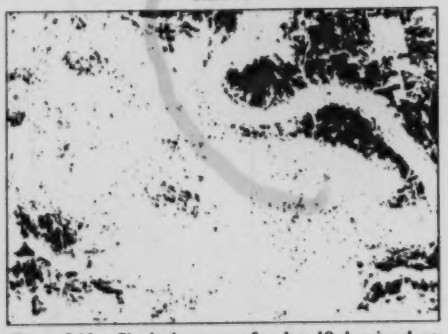

Figure 5.12a. Single theme map for class 10 showing dune-free prairie grasslands.

Class 11

Figure 5.13a. Single theme map for class 11 showing asphalt roads, exposed bedrock, and some blow-out dune areas.

Class 12

Figure 5.14a. Single theme map for class 12 showing vegetation associated with a thin soil layer and near soil bedrock exposure.

Class 10

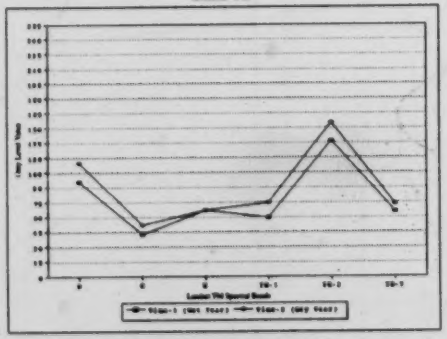

Figure 5.12b. Mean grey level values for the wet year and the dry year for raw data comprising class 10.

Class 11

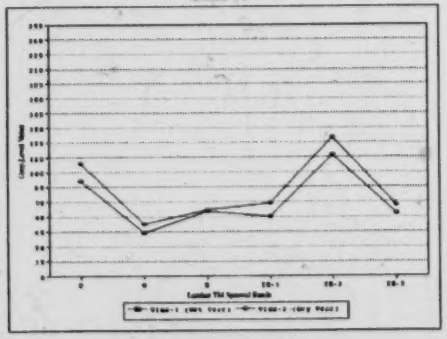

Figure 5.13b. Mean grey level values for the wet year and the dry year for raw data comprising class 11.

Class 12

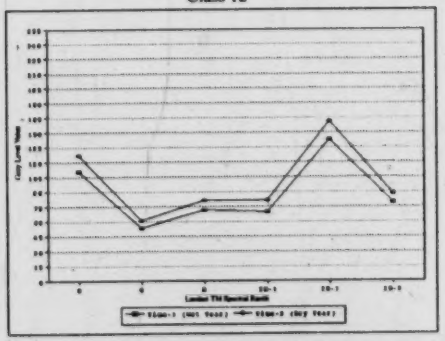

Figure 5.14b. Mean grey level values for the wet year and the dry year for raw data comprising class 12.

Class 13

Figure 5.15a. Single theme map for class 13 showing irrigated areas.

Class 14

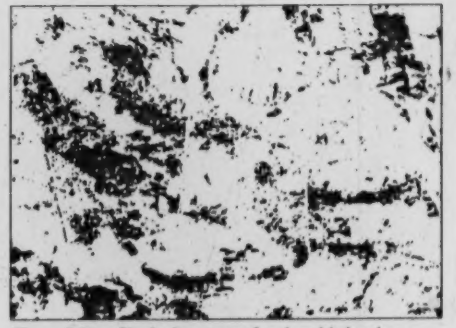

Figure 5.16a. Single theme map for class 14 showing vegetation associated with interdune areas and cereal crops.

Class 15

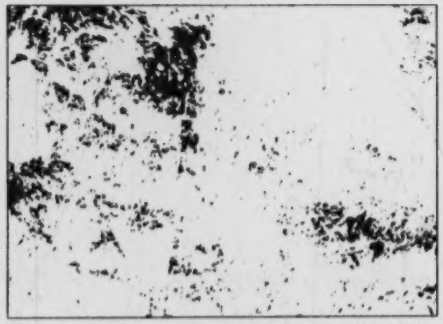

Figure 5.17a. Single theme map for class 15 showing the aeolian deposits associated with vegetation.

Class 13

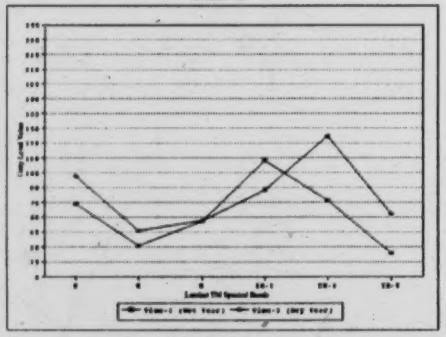

Figure 5.15b. Mean grey level values for the wet year and the dry year for raw data comprising class 13.

Class 14

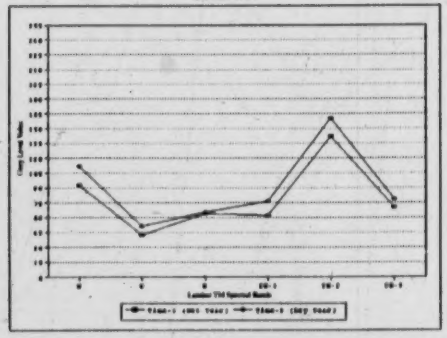

Figure 5.16b. Mean grey level values for the wet year and the dry year for raw data comprising class 14.

Class 15

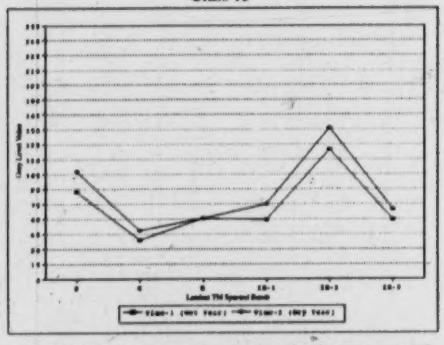

Figure 5.17b. Mean grey level values for the wet year and the dry year for raw data comprising class 15.

mean-signature graphs were created. The mean-signature graphs show the mean grey level value associated with each band for the wet year (time 1) and the dry year (time 2).

Analysis

Interpretation of surface features was based on GLV which is controlled by brightness which is not a direct measure of reflectance. Features such as rivers and lakes (Figure 5.3a) have low GLV in the infrared bands and high GLV in the visible bands. For example, Class 1 (Figure 5.3b) has high mean GLV in TM1 (blue), TM2 (green), and TM3 (red) and low mean GLV in TM4, TM5, and TM7 (the infrared bands). Features such as creeks, roads, exposed to near-exposed bedrock, and dune blow-out areas greater or equal to $30m^2$ (Classes 11 and 12) have moderate to high mean GLV in the visible bands with low mean GLV in the infrared wavelengths except for TM5 (infrared 2). For example, Class 11 (Figure 5.13) has higher mean GLV in TM1 (blue) than TM4 (infrared 1) or TM7 (infrared 3) but displays the highest mean GLV in TM5 (infrared 2). Also for Class 11 there is a small difference in GLV for TM5 (infrared 2) between the wet and the dry year due to exposure increases in the dry year and exposure decreases in the wet year. Class 9 (Figure 5.11) also has high GLV in the visible bands (mainly in TM1-blue) and higher GLV in TM5 (infrared 2). Class 9 is unique as a mean GLV difference greater than 50 occurs in TM3 (red) due to a change from dry to moist conditions.

Vegetation generally has high GLV in the infrared bands and low GLV in

the green and red bands. This is apparent for Classes 2 (Figure 5.4), 3 (Figure 5.5), 4 (Figure 5.6), 5 (Figure 5.7), 6 (Figure 5.8), 7 (Figure 5.9), 8 (Figure 5.10), 10 (Figure 5.12), 12 (Figure 5.14), 13 (Figure 5.15), 14 (Figure 5.16), and 15 (Figure 5.17). For example, Class 3 (Figure 5.5b) has higher mean GLV in TM4, TM5, and TM7 (infrared bands) than in TM2 (green) or TM 3 (red). Interestingly, the GLV of TM1 (blue) for all vegetation classes range from a GLV of 75 to a GLV of 125. According to Lillesand and Kiefer (1994), the blue band is useful in soil/vegetation discrimination and forest type mapping. Range differences between all vegetation classes for TM1 (blue) and TM4, TM5, and TM7 (infrared bands) aid in distinguishing one vegetation class from another.

Differences between each vegetation class are due to temporal variation (species moisture preferences), different species types, or soil vegetation mixtures (density variation). For example a mean infrared temporal difference of at least 30 GLV occurs in Class 6 (Figure 5.8) where the largest infrared difference is shown in TM5. The temporal variations between the wet and the dry year for Class 6 suggest that vegetation in these areas is affected by moisture variation. Vegetation classes that exhibit no temporal differences are classed separately due to the co-existence of several types of vegetation species with different spectral characteristics or the soil vegetation mixture (*i.e.* vegetation on dune crest areas is less dense than vegetation in dune trough areas).

From analysis of the fifteen single-theme maps (Figures 5.13 to 5.17), corresponding multitemporal mean-signature graphs, and a classed colour

composite (Figure 5.18), aeolian deposits (dune areas, interdune areas, and sand sheet areas) are represented by Classes 3, 4, 14, and 15. Class 4 represents dune trough vegetation and Class 3 represents dune crest vegetation where dune trough vegetation occupies a larger area than dune crest vegetation. The multitemporal mean-signature graphs show that the main difference in reflectance between Class 3 and Class 4 is in TM5 where the mean GLV in Class 3 for both dates is lower than the mean GLV in Class 4. Large temporal variations between bands for Classes 3 and 4 do not exist. This suggests the vegetation types are spectrally different and are possibly distinguishable because dune crest vegetation is less dense than dune trough locations. Class 14 and class 15 differ from classes 3 and 4 because there are mean GLV differences in TM7 (infrared 3) from time 1 to time 2 that are not present in Classes 3 and 4. Class 14 has a higher mean GLV in TM5 (infrared 2) and TM7 (infrared 3) than Class 15. Interdune area vegetation (Class 14) is different from dune trough and dune crest vegetation because topographic relief in interdune areas is low. Dune vegetation preferring moderate to low relief (Class 15) gradually merges into the interdune and prairie grassland areas.

Four classes (Classes 2, 5, 6, and 7) represent the vegetation associated with the rivers, lakes, and creeks within the Duchess dune field. Of these classes, Class 6 is the most distinguishable due to temporal variation (at least 30 mean GLV) in TM4, TM5, and TM7 (infrared bands). Classes 2, 5, and 7 show some temporal variation between the wet and the dry year, yet this variation is not as

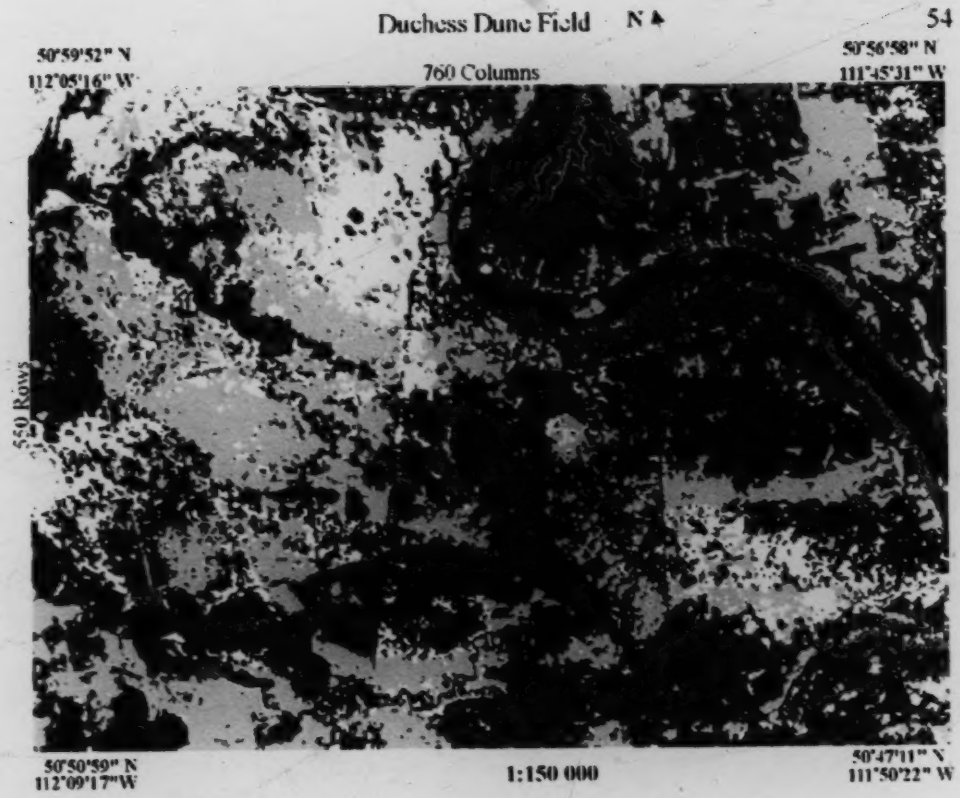

LEGEND

- Red Deer River and lakes (Class 1)
- Floodplain vegetation (Class 2)
- Aeolian dune crest location (Class 3)
- Aeolian dune trough location (Class 4)
- Vegetation in moderately low relief areas (Class 5)
- Vegetation associated with gradually sloping terrain (Class 6)
- Vegetation associated with valley sides of the Red Deer River and lakes (Class 7)
- Irrigated area appearing in the wet and the dry year (Class 8)
- Saline deposits (Class 9)
- Dune-free prairie grasslands (Class 10)
- Asphalt roads, exposed bedrock and some blow out areas (Class 11)
- Vegetation in thin soil layer and near-bedrock exposure locations (Class 12)
- Irrigated areas appearing mainly in the wet year (Class 13)
- Interdune area and cereal crops (Class 14)
- Vegetation associated with aeolian deposition in low relief areas (Class 15)

Figure 5.18. Map of the Duchess dune field with 15 classes (based on cluster analysis and discriminant analysis results).

great as Class 6. For example, the greatest mean TM5 (infrared 2) difference (approximately 15 GLV) occurs in Class 5. Mean GLV in TM1 (blue), TM2 (green), and TM3 (red) wavelengths is similar for Classes 2, 5, and 7. Differences for these classes occur in the infrared bands where; 1. Class 2 has similar mean GLV in TM4 (infrared 1) and TM5 (infrared 2) in both time periods whereas Classes 5 and 7 show higher mean GLV in TM5 (infrared 2) than TM7 (infrared 3), 2. Class 2 has lower mean GLV in TM7 (infrared 3) than classes 5 or 7 where Class 5 has higher mean GLV in the infrared bands than Class 7, and 3. Class 5 shows higher mean GLV in all bands than Class 7. These mean GLV differences suggest the presence of a variety of species adapted to specific areas and areas of of varying vegetation cover. Class 2 represents floodplain vegetation (low-lying area in close proximity to rivers and lakes), Class 5 represents vegetation growing in moderate to low relief areas often surrounding the river and creeks, and Class 7 represents vegetation growing on river slopes and higher elevated areas.

Two classes (8 and 13) represent vegetation in center pivot irrigation areas which are displayed as circles on Figures 5.10a, 5.15a, and 5.18. The multitemporal mean-signature graphs for these classes (Figures 5.10b and 5.15b) differ as greater temporal variation occurs in Class 13. For example, mean GLV in TM4 (infrared 1) for Class 13 differs by 30 between the wet and the dry year, mean GLV in TM5 (infrared 2) differs by 70, and mean GLV in TM7 (infrared 3) differs by approximately 40. In comparison, the maximum mean GLV difference occurring in TM4, TM5, and TM7 (infrared bands) for Class 8 is 20. Class 13

represents irrigated areas that are affected by increased soil moisture. This causes previously irrigated areas to stand out and results in an increase in the number of irrigated areas for Class 13.

Classes 11 (roads, exposed bedrock, and some blow-out areas) and 12 (vegetation associated with a thin soil layer and near-bedrock exposure) exhibit higher mean GLV in TM1 (blue) for both time 1 and time 2 than any other class. This results in a clear distinction of Classes 11 and 12 from all the other classes. Class 11 shows moderate mean GLV in TM5 (infrared 2) because vegetation is present in the road ditches and along the creeks. Class 12 has lower mean GLV in TM5 (infrared 2) than Class 11 because the thin soil layer, near-exposed bedrock, and blow-out dune areas are surrounded by vegetation.

Classes 1, 9, and 10 are distinct from all other classes due to their differences in mean GLV. Class 1 (rivers and lakes) is distinct from all other classes as the highest mean GLV is seen in TM1 (blue), with all other bands exhibiting the lowest mean GLV. This occurs because longer wavelengths (*i.e.* TM5-infrared 2) can not penetrate water thereby exhibiting zero to low GLV. The blue band though, is the shortest visible wavelength and is often used in water penetration studies (Lillesand and Kiefer 1994). Class 9 (saline areas) is distinct from all other classes because it has the highest mean GLV in TM1 (blue) than all the other classes. There is also a mean GLV difference of at least 50 in TM3 (red) between the wet year and the dry year. This occurs because salinity conditions are affected by moisture increases and

decreases. Class 10 (dune-free prairie grasslands) shows small temporal variations from the wet to the dry year. The multitemporal mean-signature graph (Figure 5.12b) closely resembles the signature graphs of the aeolian deposit classes but is separate because a different vegetation type is present on non-sand covered surfaces than sand covered surfaces.

A map of the Duchess dune field (Figure 5.19a) was generated by merging the original 15 classes into 7 classes. Three of the aeolian deposit classes (3, 4, and 15) were merged into one class representing vegetation associated with aeolian dunes. The other aeolian deposit class (Class 14) was unaltered as it represents the interdune and sand sheet areas that Mulira (1986) did not map. All the classes displaying river vegetation (Classes 2, 5, 6, and 7) were merged into one category which appear khaki in colour. The irrigated classes (Classes 8 and 13) were merged due to their similarity and appear pink. Classes 9, 11, and 12 were merged to represent roads, exposed to near-exposed bedrock, and dune blow-outs (light blue on map). Class 10 representing prairie grasses associated with non-sandy covered surfaces was unaltered as this area is mainly dune-free. Class 1 representing the Red Deer River, lakes, and the creeks was unaltered due to its distinct difference from all other classes.

This Duchess dune field map produced using satellite data not only shows sand sheet areas which Mulira (1986) did not map, but, also effectively defines boundaries between aeolian and non-aeolian material. In comparison with Shetsen's (1987) map a larger interdune area is present and the boundaries

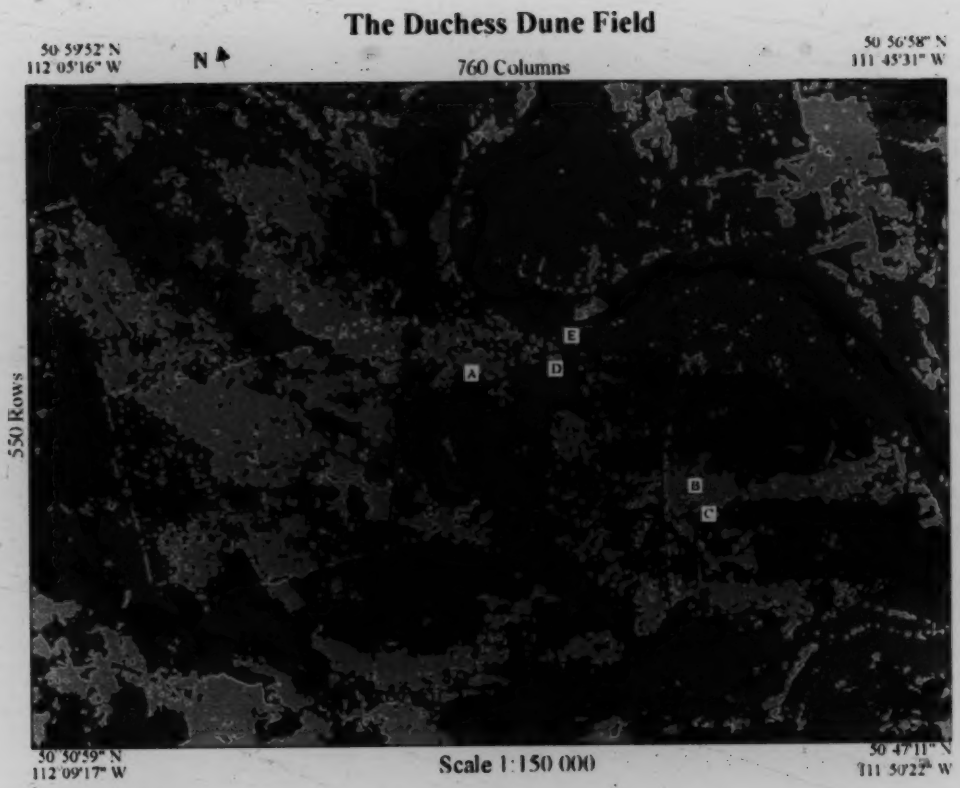

Legend

- Aeolian dunes associated with grasses, forbs, and low shrubs
- Interdune and sand sheet areas associated with tall grasses and cereal crops
- Irrigated areas
- Vegetation associated with rivers, lakes, and creeks and similar high water tables
- Asphalt and gravel roads and exposed to near-exposed bedrock
- Rivers and lakes
- Dune-free prairie grassland

Figure 5.19a. Classified map of the Duchess dune field created using multitemporal Landsat TM data obtained for a wet period and a dry period. Areas `A' to `E' correspond to ground photo and oblique aerial photo locations.

of the three main dune areas are more defined. The spectral variation within each class aided in describing differences between classes and also helped to determine aeolian from non-aeolian boundaries. The areas covered by aeolian dunes and interdune areas in the Duchess dune field are 140.5 km^2 and 84.2 km^2 respectively (determined using the program COUNT in TERRA FIRMA).

Ground truthing

Field checking was conducted before, during, and after the interpretation and merging of categories. Ground photos and oblique aerial photographs of the study area, assisted in labelling of the classes in the final map. Figure 5.20 (corresponds to area 'A' on Figure 5.19a), an area of aeolian dune deposition (see area 1), consists of Classes 3 and 4 (dune trough and dune crest locations). The blow-out area (see area 2) can be seen on the satellite map because it is greater than 30m^2 in areal extent. Not all blow-outs in the study area are identifiable on the satellite map because their small number and restricted size prevent them from being classed separately. This exemplifies the present day scale-resolution trade-off between aerial photography and satellite mapping.

Dune trough vegetation is spectrally different from dune crest vegetation because trough vegetation is greener and more dense (see area 2 on Figure 5.21). Dune crest vegetation is dominated by grasses with more sparse coverage (see area 1 on Figure 5.21). Interdune vegetation (Class 14) and dune vegetation (Classes 3 and 4) are spectrally different resulting in separate classes.

The change in vegetation cover from interdune to dune locations (Figure 5.22)

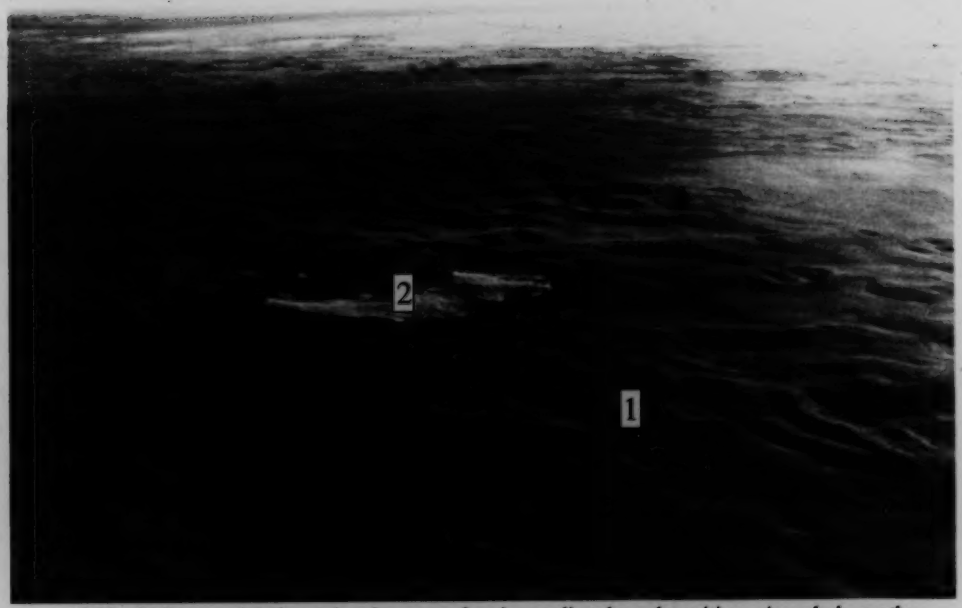

Figure 5.20. Oblique aerial photo showing area of major aeolian dune deposition. Area 1 shows the aeolian dunes and area 2 is a blow-out area. Wind direction at time of dune formation was from the northwest (top left corner).

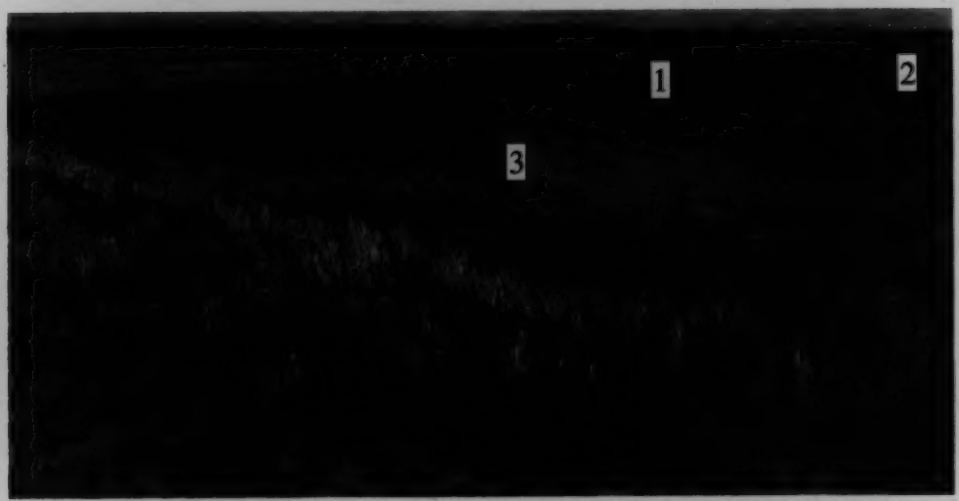

Figure 5.21. Ground photo of dune crest (area 1) and dune trough (area 2) vegetation with central blow-out (area 3) area.

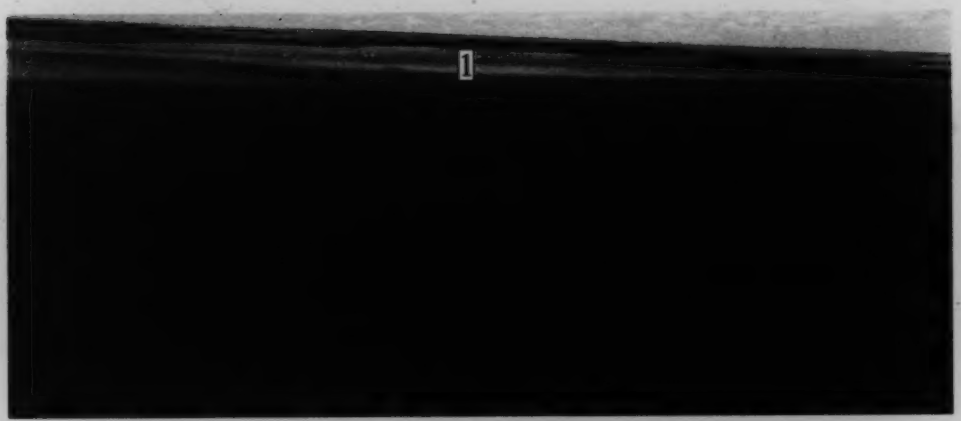

Figure 5.22. Ground photo showing the difference between dune vegetation and interdune vegetation. The colour change in area 1 shows the transition from dune to interdune areas.

Figure 5.23. Oblique aerial photo showing floodplain vegetation (area 1), dense tree cover (area 2), exposed to near-exposed bedrock (area 3), and the Red Deer River (area 4).

was photographed from area 'B' on Figure 5.19a. The interdune area (see area 1 on Figure 5.22) is dominated by light green vegetation that is occupied mainly by a few grass species. The progression from dune to interdune areas shows a colour change from dark to light green.

Riverside vegetation (Classes 2, 5,6, and 7), the Red Deer River (Class 1), and bedrock (Class 11 and 12) are shown on Figure 5.23. These features were manually separated after the cluster analysis because of their apparent physical differences. Floodplain vegetation (Class 2) consists mainly of grasses with sparse tree cover (see area 1 on Figure 5.23) and higher elevated areas along the river consist of dense tree cover (see area 2 on Figure 5.23). Figure 5.24 is a ground photo showing dense river vegetation (Figure 5.24). The river and the lakes were not classed separately because they both have the same spectral characteristics (compare Figure 5.23 to Figure 5.25). The vegetation in the lake area (Figure 5.25) is similar to the vegetation along the river and creeks which is why all river and lake vegetation classes were merged into one.

Center pivot irrigation areas (Classes 8 and 13) shown in Figure 5.26 appear as circles on the satellite map (see area 'D' on Figure 5.19a). Two irrigation classes occurred because Class 13 had a greater number of irrigated areas when compared to Class 8. The vegetation of the dune-free prairie grassland areas is classed separately because it is associated with non-sandy deposits (Figure 5.27 which corresponds to area 'E' on Figure 5.19). A ground photo (Figure 5.28) suggests, in this instance, a high gravel content.

Figure 5.24. Ground photo of dense river vegetation (corresponds to area 2 on Figure 5.23).

Figure 5.25. Oblique aerial photo of lakes and associated vegetation.

Figure 5.26. Oblique aerial photo of a center pivot irrigation system.

Figure 5.27. Dune-free prairie grasslands associated with non-sandy deposits.

Figure 5.28. Ground photo of gravel covered, dune-free prairie grassland vegetation areas.

CHAPTER 6 SUMMARY

David (1977) suggested that aeolian deposition in the prairies is affected by variations in surface moisture content and the vegetation's response to these varying moisture conditions. By purposely selecting Landsat TM data from a wet period and a dry period, it was possible to differentiate between aeolian and non-aeolian deposits. Twelve bands of TM data, six representing a wet period and six representing a dry period were used to map aeolian deposits within the Duchess dune field in southern Alberta.

Interpretation of multitemporal TM composites can be complicated because several bands of data are used in the analysis. To reduce the number of bands (six for the wet period and six for the dry period), a Principal Components Analysis (PCA) was performed. PCA results indicated that the information of the first three principal components (85.61%) was not sufficient in determining dune boundaries and that temporal differences (those containing the most variance) mainly occurred in principal components 4, 5, and 6. A principal component colour composite assigning principal component 4 to the red gun, principal component 5 to the green gun, and principal component 6 to the blue gun effectively showed dune boundaries and dune shape. PCA results suggested that moisture variation is important to consider when mapping dunes.

In addition to PCA, image classification was used to include all temporal and spectral data. Using unsupervised training field sampling (cluster analysis) and classification procedures (discriminant analysis), all pixels from all twelve

bands of data were assigned to a class. This resulted in a multitemporal image with fifteen classes. Analysis of this image, in conjunction with multitemporal mean-signature graphs, aided in manually merging these fifteen classes into seven. The final classified map with seven classes showed that the Duchess dune field consists mainly of dunes, sand sheets, and interdune deposits.

Using satellite data to map aeolian deposition has proved to be a useful tool in providing detailed information about arid environments and the effects of variations in moisture regimes. The dune and interdune boundaries present on the satellite map differ from those mapped by Shetsen (1987); she identified three main areas of aeolian deposition but did not separate these deposits into dune and interdune areas. Further to this, the satellite map allowed for the identification of sand sheet areas which Mulira (1986) does not map using aerial photos and field survey information. Satellite images are more useful in mapping the dynamic nature of arid environments and are more effective in distinguishing naturally occurring boundaries between surface features than other techniques used to date.

REFERENCES

Adams, J., Rogers, R.H., Walsh, M., and Reinhold, R. 1980. Evaluation of Multidate Data for Water Quality Modeling Application, ASP 46th Annual Meeting, St. Louis, MO, March 9-14.

Anderson A.T., Schultz, D., Buchman, N. and Nock, H.M. 1977. Landsat Imagery for Surface-Mine Inventory, *Photogrammetric Engineering and Remote Sensing*, Vol. 43, No. 8, pp. 1027-1036.

Badhwar, G.K., Austin, W.W., and Carnes, J.G. 1982. A Semi-Automatic Technique for Multitemporal Classification of a Given Crop Within a Landsat Scene, *Pattern Recognition*, Vol. 15, No. 3, pp. 217-230.

Bagnold, R.A. 1941. *The Physics of Blown Sand and Desert Dunes*. (Methuen & Co., London).

Bryan, R.B, Campbell, I.A., and Yair, A. 1987. Postglacial Geomorphic Development of the Dinosaur Provincial Park Badlands, Alberta, *Canadian Journal of Earth Sciences*, v. 24, pp. 135-146.

Byrne G.F, Crapper, P.F., and Mayo K.K. 1980, Monitoring Land-Cover Change by Principal Component Analysis of Multitemporal Landsat Data, *Remote Sensing of Environment*, 10, pp. 175-184.

Crocker, L.D. and Stone Soup Group 1990. *PICLAB*, a display package, Pittsburg, California, U.S.A.

David, P.P. 1977. *Sand Dune Occurrences of Canada*, Indian and Northern Affairs, National Parks Branch, Ottawa, pp. 1-182.

Deutsch, M. 1976. Optical Processing of ERTS Data for Determining Extent of the 1973 Mississippi River Flood in ERTS-1, *A New Window on Our Planet*, U.S. Government Printing Office, Washington, D.C., pp. 209-213.

Dwivedi, R.S. and Sankar, R.V. 1992. Principal Component Analysis of Landsat MSS Data for Delineation of Terrain Features, *International Journal of Remote Sensing*, Vol. 13, No. 12, pp. 2309-2318.

Dyke, A.S. and Prest, V.K. 1987. *Late Wisconsinan and Holocene Retreat of the Laurentide Ice Sheet*, Map 1702 A, 1: 5 000 000, Geological Survey of Canada.

Eastman, J.R., 1993. *IDRISI*, a grid-based Geographic Analysis System, Clarke University.

Environment Canada 1994. Mean Monthly Temperature (°C) for Alberta.

Environment Canada 1994. Year-Month Matrix for Total Precipitation (mm) for Alberta.

Environment Canada 1994. Monthly Wind Data (km/hr) for Alberta.

Eyton, J.R. 1983. Landsat Multitemporal Color Composites, *Photogrammetric Engineering and Remote Sensing*, Vol. 49, No. 2, pp. 231-235.

Eyton, J.R. 1992. *TERRA FIRMA*, a cartographic display package, University of Alberta, Edmonton, Alberta.

Gillieson, D.S., Cochrane, J.A., and Murray, A. 1994. Surface Hydrology and Soil Movement in an Arid Karst: the Nullarbor Plain, Australia, *Environmental Geology*, 23, pp. 125-133.

Howarth, P.J. and Wickware G.M. 1981. Procedures for Change Detection Using Landsat Digital Data, *International Journal of Remote Sensing* 2, pp. 277-291.

Jacobberger, P.A. 1989. Reflectance Characteristics and Surface Processes in Stabilized Dune Environments, Remote Sensing of Environment. 28; April-June, 287-295.

Jacobberger, P.A. and Hooper D.M. 1991. Geomorphology and Reflectance Patterns of Vegetation-covered Dunes at the Tsoldilo Hills, North-west Botswana, *International Journal of Remote Sensing*, 12: 11, 2321-2342.

Johnston, R.J. 1978. *Multivariate Statistical Analysis in Geography*, John Wiley & Sons Inc., NY.

Kjearsgaard, A.A., Peters, T.W., and Pettapiece, W.W. 1983. *Soil Survey of the County of Newell, Alberta*, Research Branch, Agriculture Canada.

Kumar M., Goossens E., and Goossens R. 1993. Assessment of Sand Dune Change Detection in Rajasthan (Thar) Desert, India, *International Journal of Remote Sensing*, Vol 14, No. 9, pp. 1689-1703.

Lam M.C.F. and Hoyt, R.R. 1972. High Speed Image Correlation for Change Detection, *National Aeronautics and Electronics Conference*, Dayton, Ohio.

Li R.Y., Fawwaz, T.U., and Eyton J.R. 1980. Crop Classification with a Landsat/Radar Sensor Combination, *Machine Processing of Remotely Sensed Data*.

Lillesand T.M. and Kiefer R.W. 1994. *Remote Sensing and Image Interpretation*. (John Wiley & Sons, Inc., U.S.A).

Luce, F.C. and Turner, B.J. 1981. Effectiveness of Using Digital Processing Techniques to Detect Temporal Change from Digitized Aerial Photographs, *U.S. Department of Defense*, Defense Mapping Agency, University Park, Pennsylvania, U.S.A.

McKee, Edwin D., and Breed, Carol S. 1974. An Investigation of Major Sand Seas in Desert Areas Throughout the World, *Goddard Space Flight Center; NASA* , Third Earth Resources Technolgy Satellite-1 Symposium, Vol 1: Technical Presentations.

Melton, Frank A. 1940. A Tentative Classification of Sand Dunes: Its Application to Dune History in the Southern High Plains, *Journal of Geology*. 28; 2, 113-172.

Mishra J.K., Joshi M.D. and Devi R. 1994. Study of Desertification Process in Aravalli Environment Using Remote Sensing Techniques, *International Journal of Remote Sensing*, Vol. 15, No. 1, pp. 87-94.

Mulira, J.E 1986. *Eolian Landforms of Alberta*, Alberta Forestry, Lands, and Wildlife, Edmonton.

Odynsky, W.M. 1958. U-shaped Dunes and Effective Wind Directions in Alberta, *Canadian Journal of Soil Science* 38, pp. 56-62.

Proudfoot W. 1994. *Climatic Change and Environmental Implications in the Medicine Hat Region Using Billings, Montana as an Analogue*, unpublished MSc., University of Alberta, Edmonton, Alberta, pp. 28-45.

Ribed P.S. and Lopez A.M. 1995. Monitoring Burnt Areas by Principal Components Analysis of Multi-Temporal TM data, *International Journal of Remote Sensing*, Vol. 16, No. 9, pp. 15-27.

Schreier, H., Goodfellow, L.C., and Lavkulich, L.M. 1982. The Use of Digital Multi-Date Landsat Imagery in Terrain Classification, Photogrammetric Engineering and Remote Sensing, Vol. 48, No. 1, pp. 111-119.

Shetsen, I. 1987. *Quaternary Geology:Southern Alberta*, 1:500,000, Alberta Research Council.

Smith, H.T.U. 1953. Classification of Sand Dunes /Abstracts/: *International Geology Congress*, 19th, Algeria, 1952.

Stauffer M.L., McKinney, R.L., and Chaikin, L.M. 1978. *Landsat Image Differencing as an Automated Land Cover Change Detection Technique*, Goddard Space Flight Center, U.S.A.

Strong, W.L. and Leggat K.R. 1992. Ecoregions of Alberta, *Alberta Forestry, Lands and Wildlife*, Edmonton, Alberta, Vol. 1, pp. 77.

Thomas, D.S.G. 1989. *Arid Zone Geomorphology* pp. 1-6 and 232-261. (John Wiley & Sons, New York, U.S.A.)

Wolf, P.R. 1974. *Elements of Photogrammetry*. (McGraw-Hill Book Company, U.S.A.).